

1 **Carbon dioxide release driven by organic carbon in minerogenic**  
2 **salt marshes**

3 Nora Kainz<sup>1</sup>, Franziska Raab<sup>1</sup>, L. Joëlle Kubeneck<sup>2,3,4</sup>, Ruben Kretzschmar<sup>2</sup>, Andreas Kappler<sup>1</sup>,  
4 Prachi Joshi<sup>1,5\*</sup>

Formatted: English (US)

5 <sup>1</sup> Department of Geosciences, University of Tübingen, Schnarrenbergstrasse 94-96, 72076 Tübingen, Germany

6 <sup>2</sup> Department of Environmental Systems Science, ETH Zürich, CHN, Universitätstrasse 16, 8092 Zürich, Switzerland

7 <sup>3</sup> Department of Microbiology, Radboud Institute for Biological and Environmental Sciences, Radboud University,  
8 6525 AJ Nijmegen, The Netherlands

9 <sup>4</sup> TNO Geological Survey of the Netherlands, PO Box 80015, 3508 TA Utrecht, The Netherlands

10 <sup>5</sup> Swiss Federal Institute for Forest, Snow and Landscape Research WSL, Zürcherstrasse 111, 8903 Birmensdorf,  
11 Switzerland

12 \*Correspondence: prachi.joshi@wsl.ch

Formatted: Left, Space After: 8 pt

13 **Abstract**

14 Coastal wetlands play an important role in the global carbon cycle by sequestering carbon (referred to as  
15 “blue carbon”). At the same time, organic carbon (OC) in the subsurface is decomposed, releasing greenhouse gases  
16 (GHGs) such as carbon dioxide (CO<sub>2</sub>) and methane (CH<sub>4</sub>). To predict how this carbon balance in salt marshes will  
17 change under future climate scenarios (e.g., higher temperatures, sea level rise), it is essential to understand the controls  
18 on OC decomposition in these systems. Here, we investigated OC turnover and CO<sub>2</sub> release in a minerogenic salt marsh  
19 at the Wadden Sea, Germany. We first characterized the porewater and sediment of a pioneer marsh and adjoining  
20 intertidal flat to identify key biogeochemical processes. We then performed an in situ experiment by injecting two OC  
21 sources (labile (acetate)/complex (humic acid)) and subsequently monitored GHG release over four injection cycles  
22 along with subsurface geochemistry. Overall, we found that electron acceptors, primarily sulfate (SO<sub>4</sub><sup>2-</sup>), were present  
23 at all tested depths and no CH<sub>4</sub> was detected, suggesting that electron acceptor availability was unlikely to be the  
24 primary limiting factor on microbially mediated CO<sub>2</sub> release; the availability of OC (concentration and composition)  
25 may rather act as a limiting factor. Following the addition of labile OC, CO<sub>2</sub> release in the pioneer marsh increased  
26 by up to 47.4 ± 36.4 % compared to the control, with a generally similar trend in the intertidal flat. The CO<sub>2</sub> release  
27 from the complex OC treatment was similar to the control. The results of our work improve understanding of  
28 minerogenic salt marsh OC dynamics in temperate zones and enable better prediction of future changes.

**Deleted:** ¶

**Formatted:** Justified, Indent: First line: 0.5", Line spacing: 1.5 lines

**Deleted:** the microbially mediated CO<sub>2</sub> release was likely limited by OC availability and composition, and electron acceptor availability was unlikely to be the primary limiting factor, as evidenced by the presence of aqueous sulfate (SO<sub>4</sub><sup>2-</sup>) at all tested depths and the lack of detectable CH<sub>4</sub>.

35

## 1 Introduction

36

37

38

39

40

41

42

43

44

45

46

47

48

49

50

51

Vegetated coastal wetlands, located at the interface between land and the open sea, occur along all continental coastal zones except Antarctica and comprise mangroves, seagrass, and salt marshes (Nellemann et al., 2009; Pendleton et al., 2012; Tan et al., 2025). Salt marshes, including the seaward adjoining intertidal flats, sequester high amounts of carbon primarily in the sediment (McLeod et al., 2011; Nellemann et al., 2009; de Vlas et al., 2013). Globally, around 60.4-70 Tg yr<sup>-1</sup> of carbon is buried in vegetated salt marshes (Duarte et al., 2005; Nellemann et al., 2009). The sequestration of carbon is disproportional in vegetated coastal areas, with around half of the total organic carbon in ocean sediment (often referred to as “blue carbon”) buried in these areas which only account for 0.2 % of the ocean surface (Duarte et al., 2013; Nellemann et al., 2009). As the rate of carbon input into the sediment exceeds its rate of decomposition (especially for allochthonous carbon), salt marshes are characterized by high carbon sequestration rates (Mueller et al., 2019; Temmink et al., 2022; Van de Broek et al., 2018). Simultaneously, salt marshes release greenhouse gases (GHGs) due to organic carbon (OC) decomposition: carbon dioxide (CO<sub>2</sub>) at 0.02-0.24 Pg CO<sub>2</sub> yr<sup>-1</sup> (Pendleton et al., 2012) and methane (CH<sub>4</sub>) at 0.142 ± 0.02 Mg carbon ha<sup>-1</sup> yr<sup>-1</sup> (Alongi, 2020). Therefore, understanding carbon turnover in coastal wetlands is crucial for predicting how these ecosystems will respond to climate change, such as temperature increase, sea level rise, and eutrophication of coastal waters. This is especially important given the annual 1-2 % loss of salt marshes due to land-use change and their vulnerability to climate impacts (Duarte et al., 2008).

52

53

54

55

56

57

58

59

60

61

62

In coastal wetlands, microbial respiration pathways couple OC as an electron donor with terminal electron acceptors (TEAs), especially oxygen (O<sub>2</sub>), ferric iron (Fe(III)) and sulfate (SO<sub>4</sub><sup>2-</sup>) (Tan et al., 2025; Tobias and Neubauer, 2019). Oxygen, the thermodynamically most favourable TEA, exhibits fluctuating penetration depth into the sediment due to tides, bioturbation or root-mediated O<sub>2</sub> transport (de Beer et al., 2005; Huettel et al., 2014; Maricle and Lee, 2002). In deeper sediment layers, where anoxic conditions can dominate, microorganisms utilize Fe(III), from iron minerals, or SO<sub>4</sub><sup>2-</sup>, which infiltrates the sediment through inundation of seawater, as alternative TEAs (Jørgensen et al., 2019; Tobias and Neubauer, 2019). Upon full depletion of TEAs, OC is further decomposed to CH<sub>4</sub> (Schlesinger and Bernhardt, 2013b). Microbial decomposition of OC may be further influenced by its chemical composition. Chemically simpler e.g., short chain aliphatic OC may be substantially favoured for decomposition compared to complex OC, such as natural organic matter (Gunina and Kuzyakov, 2022; Lipczynska-Kochany, 2018; Schlesinger and Bernhardt, 2013a).

63

64

65

66

67

68

69

70

71

The primary controls on GHG release in salt marshes, as interfaces between land and open ocean, are not fully understood. Specifically, it is unclear whether OC turnover is primarily controlled by the availability of the electron acceptors – as observed in organogenic marshes and consistent with studies in terrestrial wetlands (Schlesinger and Bernhardt, 2013b) – or by the organic matter itself, as suggested for marine sediment in general (Arndt et al., 2013). Past studies on OC dynamics (including GHG release) in salt marshes have largely concentrated on the eastern coast of the US (Capooci et al., 2024; Kostka et al., 2002b; Lowe et al., 2000; Seyfferth et al., 2020), which is dominated by organogenic peat marshes. Organogenic marshes are generally low energy, microtidal wetlands, characterized by a high organic matter deposition via autochthonous pathways that results in high TOC contents (Logemann et al., 2025). For example, Lowe et al. (2000) and Kostka et al. (2002a) observed that OC oxidation was controlled by SO<sub>4</sub><sup>2-</sup> and

Deleted: .....Page Break.....

Field Code Changed

74 Fe(III) reduction in salt marshes in Georgia, USA. Further, CH<sub>4</sub> fluxes were detected in salt marshes in Delaware,  
75 suggesting a co-occurrence of methanogenesis and SO<sub>4</sub><sup>2-</sup> reduction (Capooci et al., 2024; Seyfferth et al., 2020).  
76 European salt marshes, in contrast, are primarily minerogenic, i.e., contain high fractions of mineral sediment due to  
77 high sedimentation rates, resulting in comparably lower TOC content (Nolte et al., 2013). Studies conducted in  
78 European salt marshes have focused on the TEA turnover (e.g., SO<sub>4</sub><sup>2-</sup> respiration rates) and not GHG emissions (de  
79 Beer et al., 2005; Bosselmann et al., 2003; van Erk et al., 2023). These studies showed that O<sub>2</sub> penetrates down the  
80 sediment, Fe(III) is available and SO<sub>4</sub><sup>2-</sup> reduction occurs. Hence, these studies have provided indirect links between  
81 belowground biogeochemistry, especially in the context of available TEA, and the release of GHGs in minerogenic  
82 salt marshes; however, a direct investigation of the determining factor(s) of OC degradation from these ecosystems is  
83 missing. By understanding the controls on GHG release, we can better predict how climate impacts such as higher  
84 temperatures and sea level rise will affect OC turnover and thereby GHG release in minerogenic salt marshes.

85 To investigate the in situ carbon dynamics in minerogenic salt marshes, we chose a representative field site  
86 at the Wadden Sea coast. Our goals were (i) to identify the key microbial processes (O<sub>2</sub>, Fe(III) and/or SO<sub>4</sub><sup>2-</sup> reduction)  
87 that control the release of OC as CO<sub>2</sub> and/or CH<sub>4</sub>, and (ii) to determine the role of OC (concentration and composition)  
88 in the release of GHGs. To this end, we first characterised the primary geochemical parameters from a minerogenic  
89 pioneer marsh and intertidal flat at the German Wadden Sea. Building on those results, we conducted an in situ  
90 manipulation experiment investigating the impact of two contrasting OC sources (acetate, humic acid) on GHG  
91 emissions. We hypothesized that (i) the high energy and sediment inputs in minerogenic salt marshes result in low  
92 TOC supply and high TEA availability. (ii) We further hypothesize that this leads to the likely limitation of electron  
93 donor and not acceptor on OC decomposition and (iii) the composition of OC plays a more important role than the  
94 concentration in CO<sub>2</sub> release from a minerogenic salt marsh. These hypotheses were tested in two successional zones  
95 of a salt marsh, a pioneer marsh with sparse pioneer vegetation and a non-vegetated intertidal flat.

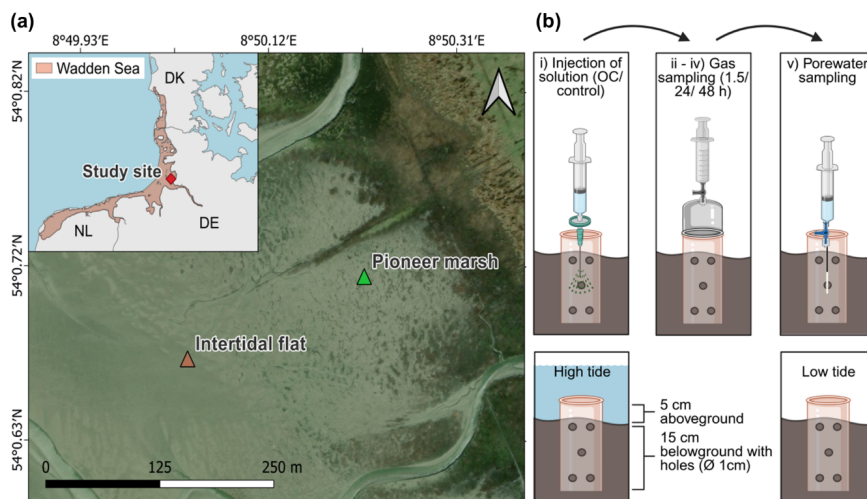
Field Code Changed

96 **2 Materials and Methods**

97 **2.1 Study site**

98 This study was conducted at the Altfelder Koog by Friedrichskoog (54°01'02.4"N 08°51'17.09"E), an area  
99 that consists of a salt marsh with different successional zones in the Wadden Sea National Park (Schleswig-Holstein)  
100 in northern Germany at the mouth of the Elbe estuary (Fig. 1a). The Wadden Sea is a UNESCO World Heritage Site  
101 and the largest continuous salt marsh (including tidal flats) in Europe (Common Wadden Sea Secretariat, 2017). The  
102 tidal range at the study area is 3.59 m, defined as the difference between mean height of high water and approximately  
103 the lowest astronomical tide. The mean high tide is 1.56 m higher than the mean sea level (BSH, 2025).

104 At the Wadden Sea, different successional zones of salt marshes are developing as a result of the ongoing  
105 process of sediment transportation by waves and tides (Esselink et al., 2017; de Vlas et al., 2013). The two successional  
106 zones which are of interest in our study are the pioneer marsh and the intertidal flat (Fig. 1a). Pioneer species such as  
107 *Salicornia* spp. and *Spartina anglica* occur in the pioneer marsh, promoting further sediment trapping (Esselink et al.,  
108 2017; de Vlas et al., 2013). The intertidal flat (seaward of a pioneer marsh) is an area with no plants to buffer incoming  
109 waves and is therefore subject to a strong tidal influence (Esselink et al., 2017). In general, both the pioneer marsh and  
110 intertidal flat are inundated daily during high tide, with the pioneer marsh experiencing less and shorter inundation (<  
111 3 h fully inundated) compared to the intertidal flat (> 3 h fully inundated) (de Vlas et al., 2013). During a spring tide,  
112 which occurs twice a month, the magnitude of high and low tide is amplified leading to stronger exposure of the pioneer  
113 marsh to tides (Gao, 2019; Kvale, 2006).



114

115 **Figure 1. Study site at the Wadden Sea including the successional zones of a salt marsh and a schematic representation of**  
 116 **the in situ experimental design.** (a) Wadden Sea, in light red in the inset with a red marker indicating our study site in northern  
 117 Germany (Friedrichskoog, Elbe estuary). Gradient of salt marsh successional zones, beginning with the intertidal flat, followed by  
 118 the pioneer marsh and more developed successional zones extending further inland. Map information: Reference system WGS 1984,  
 119 UTM 32N, data imagery ESRI 2025. (b) Experimental design: experimental procedure (top) and cylinder setup in sediment (below).  
 120 Each sampling plot consisted of a 20 cm long cylinder (diameter 16 cm), drilled with 1 cm diameter holes along the length of the  
 121 cylinder. The cylinder was inserted 15 cm deep in the sediment to define the injection area. The top 5 cm was used to mount a gas  
 122 chamber during gas sampling. The cylinder stayed in the sediment over the course of the experiment including high and low tide.  
 123 Numbers i-v indicate the experimental procedure: i) injection of solution (acetate or humic acid, only NaCl for control), ii) 1.5 h  
 124 after injection, the first gas measurement was done, iii) followed by the second gas measurement after 24 h of injection, and iv) the  
 125 final gas measurement after 48 h of injection, followed by the final step of v) porewater sampling. Each treatment (acetate, humic  
 126 acid) and the control consisted of spatial triplicates.

## 127 2.2 Porewater and sediment sampling for general geochemistry

128 In August 2022 and 2023, sediment cores were collected from the pioneer marsh and intertidal flat to analyse  
 129 the general geochemistry of the sediment and porewater. The sampling was performed during low tide. Push cores  
 130 were collected using core liners (UWITEC, polyvinyl chloride PVC) with an inner diameter of 8.6 cm (outer diameter  
 131 9 cm) and a length of 60 cm. To minimize compression, we used open push cores and only capped them when the core  
 132 liner was fully in the sediment. Furthermore, the inside wall of the cores was plain and clean to smoothly insert the  
 133 core liner in the sediment. To further minimize disturbance, the sampled cores were immediately closed, vertically  
 134 transported, and stored in the dark. At depth intervals of 5 cm, porewater samples (Rhizon sampler CSS, 0.12-0.18  $\mu$ m  
 135 pore size, Rhizosphere Research, Netherlands) and sediment samples (using a cut-off syringe) were taken through  
 136 pre-drilled holes which had been covered with isolation tape during coring. We made sure to not take sediment or

137 porewater samples at the edges but rather from the middle of the cores, where the sediment is likely undisturbed.  
138 Porewater samples were analysed for dissolved organic carbon (DOC), iron speciation,  $\text{SO}_4^{2-}$ , and dissolved  $\text{CH}_4$ , and  
139 sediment samples for total organic carbon (TOC). Detailed method for dissolved  $\text{CH}_4$  sampling is given in Supplement,  
140 S1.1.

141 We collected further sediment cores for fine scale  $\text{O}_2$  profiles. For this, sediment push cores (inner diameter  
142 2.5 cm, length 10 cm) were collected and immediately sealed. Shortly after sampling,  $\text{O}_2$  profiles were taken with a  
143 depth resolution of 500  $\mu\text{m}$  using Clark-type  $\text{O}_2$  microsensors (Unisense, Denmark) with a 100  $\mu\text{m}$  tip, following  
144 Revsbech (1989). Before measurement, a two-point calibration was done using air-saturated seawater and 0.1 M  
145 sodium ascorbate in 0.1 M NaOH solution. Profiles were recorded with the Unisense software SensorTrace Suite  
146 (version 2.8.200.21688, Unisense, Denmark).

### 147 **2.3 Physicochemical characteristics of the sediment**

148 For a general physicochemical characterization, bulk sediment was collected from a depth up to 15-20 cm in  
149 sterile sample bags with puncture proof tabs (Nasco, Whirl-pak, USA), and stored at 4 °C in the dark. Stones and  
150 macrofauna were removed prior to further analysis. We determined grain density, bulk porosity, moisture content, and  
151 particle size (details in Supplement, S1.2).

### 152 **2.4 In situ experiment: Enhanced organic carbon input**

#### 153 **2.4.1 In situ experiment design**

154 An in situ OC addition experiment was conducted in August and September 2023 to test the response of  
155 pioneer marsh and intertidal flat systems to elevated inputs of OC with different compositions. We choose acetate, a  
156 chemically simple organic compound that has been detected at other salt marshes (Hyun et al., 2007; Kostka et al.,  
157 2002a) and at a site nearby (Llobet-Brossa et al., 2002), and humic acid (in the form of Pahokee Peat humic acid), a  
158 more complex OC source, as a proxy for natural organic matter. The two OC sources were chosen, knowing their  
159 thermodynamical difference from previous studies (Gunina and Kuzyakov, 2022), to present a fermentation product  
160 (acetate) and a proxy for terrestrial organic matter (in addition to the difference with respect to complexity). Studying  
161 both labile and complex OC additions is ecologically relevant as salt marshes receive OC from multiple sources  
162 (Howard et al., 2023; Temmink et al., 2022). Eutrophication of coastal waters and/or root exudates can supply readily  
163 degradable OC to salt marshes, while increased organic matter load in rivers can deliver more complex OC compounds  
164 to salt marshes. The applied OC compounds in our study, therefore, represent environmental scenarios and allows us  
165 to investigate how these OC sources influence GHG release under realistic conditions. The injection solutions were  
166 prepared in the laboratory prior to use in the field. Solutions of 1 g OC  $\text{L}^{-1}$  were prepared with either acetate or humic  
167 acid as a carbon source. For the preparation of the solutions, sodium acetate or Pahokee Peat humic acid (obtained  
168 from the International Humic Substances Society (IHSS), Table S1) were dissolved in deionized water (Barnstead MQ  
169 system, Thermo Fisher Scientific, Germany), the pH was adjusted to 7.07-7.81 and NaCl was added (20 g  $\text{L}^{-1}$ ). The  
170 solution for the control only contained NaCl. Additionally, 25 mM bromide ( $\text{Br}^-$ ) (in the form of NaBr) was added into

171 the carbon and control solutions as an inert tracer in the field. All solutions were purged with nitrogen and stored at 4  
172 °C in the dark until used in the field. Details of the preparation process are provided in Supplement, S1.3.

173 The in situ experiment was performed in the pioneer marsh (54°00'43.14"N 08°50'12.9"E) and intertidal flat  
174 (54°00'40.45"N 08°50'02.27"E) (Fig. 1a), with the same setup in both zones. The assigned plots in the field were  
175 selected as visually similar triplicates (spatial triplicates), at a distance of ~5 m between plots of the same treatment  
176 and ~10 m between different treatments and the control plots. In the pioneer marsh, plots were placed outside of  
177 vegetated areas, i.e., the actual plot area of injection and sampling were free of vegetation although vegetation was  
178 present in the vicinity (Figs. S1a/b). For the intertidal flat, no vegetation was present, neither in the surroundings nor  
179 inside of the plots (Figs. S1c/d). Each plot consisted of a 16 cm diameter PVC cylinder with both ends open which  
180 was pushed 15 cm deep into the sediment (Fig. 1b). Holes (diameter 1 cm) were drilled in the cylinder wall to allow  
181 underground water movement. A porewater sampler (Rhizon sampler CSS, 0.12-0.18 µm pore size, Rhizosphere  
182 Research, Netherlands) was inserted in the middle of each plot at a depth of 5-10 cm and remained in the sediment  
183 over the duration of the experiment. The cylinder reached 5 cm out of the sediment, allowing a gas flux chamber to be  
184 mounted gastight for gas measurements. During the experiment, the cylinder stayed in the field. To decrease the  
185 influence of disturbances due to the setup of the experiment, we waited at least three days between setting up and the  
186 first measurements. Apart from the incubation time for gas sampling, the sediment within the cylinder was exposed to  
187 the atmosphere (low tide) or covered with seawater (high tide) (Fig. 1b).

188 The experiment was conducted similarly in both zones, the pioneer marsh and intertidal flat, using spatial  
189 triplicates and comprising four injection cycles (Fig. 1b). One injection cycle consisted of i) the injection of the anoxic  
190 sterile solution (OC or control solution), followed by ii) the first gas sampling 1.5 h after the injection. Gas sampling  
191 was repeated iii) 24 h after the injection and iv) 48 h after the injection. After the 48 h gas sampling, v) porewater was  
192 collected. Injection of the solutions and sampling was done during low tide. The solution for the different treatments  
193 was slowly injected in step i) with a bent needle at a depth of approximately 5-10 cm in the middle of each plot into  
194 the sediment. The injected solution was filtered (PES filter, pore size 0.22 µm, pre-rinsed with double deionized water)  
195 during injection to ensure that the solutions were sterile.

196 In each injection cycle, the native OC was increased by 12.0 mg C L<sup>-1</sup> in the pioneer marsh and 12.6 mg C L<sup>-1</sup>  
197 in the intertidal flat, assuming an even distribution across the experimental cylinder (calculation Supplement, S1.4).  
198 After one cycle was completed, the system had three days to recover before the next injection. At the end of the four  
199 injection cycles, sediment samples were collected (details below). The applied approach allowed us to assess short-  
200 term OC process response in minerogenic salt marshes, rather than long-term responses.

## 201 **2.4.2 In situ experiment sampling**

### 202 **Gas sampling**

203 Gas sampling was conducted using an opaque, static, non-flow gas chamber made of polypropylene (chamber  
204 volume 3000 cm<sup>3</sup>). The gas chamber was placed on the cylinder and gas samples were collected at 20-minute intervals  
205 over an incubation period of 1 hour using a 50 mL gastight syringe with a three-way valve. For sampling, the chamber

206 gas was gently mixed by pumping the syringe plunger three times before withdrawing 35 mL gas. The first 5 ml were  
207 used to flush the attached needle, and the rest was transferred immediately into a pre-evacuated 12 mL Exetainer® vial  
208 (Labco, UK). The samples were measured with a Greenhouse GC equipped with two Pulsed Discharge Detector (PDD)  
209 (ThermoFisher Scientific TRACE™ 1310 GC-Analyzer, USA – custom designed by S+H-Analytik) and two column  
210 structure (first structure 30 m long, 0.53 mm ID TGBondQ column, second structure 30 m long, 0.53 mm ID Molsieve  
211 column (for CH<sub>4</sub>) and 30 m long 0.32 mm ID TGBondQ+ column (for CO<sub>2</sub>, N<sub>2</sub>O)). Calculation for the gas fluxes and  
212 cumulative CO<sub>2</sub> emissions are given in Supplement, S1.5.

### 213 **Porewater sampling**

214 Porewater samples were collected via the pre-installed porewater sampler. The pH (Mettler Toledo SevenGo,  
215 Germany) and salinity (refractometer) were measured in the field. The collected porewater was fixed for DOC  
216 (acidification with 2 M HCl), iron speciation (acidification with 1 M HCl), and total sulfide (S(II)<sub>tot</sub>) (alkalinization  
217 with zinc acetate). Dissolved inorganic carbon (DIC) samples were transferred into vials without headspace  
218 immediately after sampling and capped. The remaining porewater was anoxically stored in nitrogen flushed bottles in  
219 the dark at 4 °C for Br<sup>-</sup>, SO<sub>4</sub><sup>2-</sup> and chloride (Cl<sup>-</sup>) measurements.

### 220 **Sediment sampling**

221 At the end of the experiment, sediment samples were collected for geochemical analysis (TOC, solid iron  
222 speciation, sulfide species) and microbial analysis. For this, push cores (inner diameter of 2.5 cm, and a length 10 cm)  
223 were taken from the middle of each plot at the same positions as the porewater samples and immediately frozen until  
224 further analysis. Sediment samples for the molecular biology analysis were stored at -80 °C upon bringing them back  
225 to the laboratory.

## 226 **2.5 Geochemical analysis**

### 227 **2.5.1 Porewater analysis**

228 DOC (as non-purgeable OC) and DIC (as the difference of total carbon and OC) was determined by a TOC  
229 analyser (multi N/C 2100S, Analytik Jena GmbH, Germany). To analyse the iron speciation in the porewater, the  
230 ferrozine assay (Stookey, 1970) was used. The S(II)<sub>tot</sub> was quantified by the Cline assay (Cline, 1969). Sulfate, Br<sup>-</sup>,  
231 and Cl<sup>-</sup> were analysed by an ion chromatograph (Metrohm 930 Compact IC Flex, Switzerland).

### 232 **2.5.2 Sediment analysis**

233 For all sediment analyses, sampled cores were thawed in an anoxic glovebox to prevent oxidation (UNILab  
234 plus Glovebox, MBRAUN, Germany), sliced in two depths (0-5 and 5-10 cm), and each depth fraction was  
235 homogenized by hand.

### 236 **Iron extraction**

237 To target the poorly and higher crystalline iron phases in the sediment samples, parallel iron extractions were  
238 performed under anoxic conditions, adapted from Moeslund et al. (1994) and Lueder et al. (2020). From each depth

239 (0-5 and 5-10 cm) ~0.2 g wet sediment sample (in triplicates) were added into an Eppendorf tube. To extract poorly  
240 crystalline iron minerals, we used an extraction with anoxic 0.5 M HCl (Heron et al., 1994). We expect that poorly  
241 crystalline iron (oxyhydr)oxides as well as ferrous iron (Fe(II)) phases such as carbonates and sulfides (e.g., FeCO<sub>3</sub> or  
242 FeS) would be extracted by this acidification. One mL of anoxic 0.5 M HCl was added to the sediment, vortexed, and  
243 incubated for 2 h in the dark at room temperature in the glovebox. For the extraction of iron minerals of higher  
244 crystallinity, targeting more crystalline Fe(II) (except pyrite) and Fe(III) phases (Cornwell and Morse, 1987; Heron et  
245 al., 1994), 1 mL of anoxic 6 M HCl was added to the sediment, and the sediment was vortexed and vertically rotated  
246 for 24 h under anoxic conditions at room temperature (30 rpm, dark). For both HCl extractions, the samples were then  
247 centrifuged (5 min, 13400 rpm), the supernatant was diluted with 1 M HCl, and iron speciation and concentration of  
248 the supernatant was determined using the ferrozine assay (Stookey, 1970). Total iron and Fe(II) concentrations of the  
249 supernatant were measured directly, and Fe(III) was determined by subtracting Fe(II) from total iron. To obtain the  
250 higher crystalline fraction separately, the poorly crystalline fraction (0.5 M HCl extract) was subtracted from the 6 M  
251 HCl fraction. We acknowledge that the weaker acid extraction extracted Fe(II) from carbonates and sulfides in addition  
252 to iron (oxyhydro)oxides. We therefore used this approach to determine the crystallinity of iron minerals and call it  
253 poorly (extracted by 0.5 M HCl) and higher (extracted by 6 M HCl) crystalline iron minerals (and not (oxyhydr)oxides).

#### 254 **Acid volatile sulfide**

255 To determine the mass of acid volatile sulfide (AVS) in the sediment similar to Burton et al. (2007), ~2 g of  
256 wet sediment was weighed in centrifuge tube in a glovebox. A smaller tube filled with anoxic 1 M zinc acetate + anoxic  
257 2 M NaOH (v/v 15:85) was placed into the sediment-filled centrifuge tube. To the sediment, 10 mL anoxic 6 M HCl  
258 + 2 mL anoxic 1 M L-ascorbic acid was added and immediately closed. The double tubes were placed in an ultrasonic  
259 bath for 30 seconds, followed by horizontal shaking overnight (150 rpm). The sulfide released from the sediment was  
260 captured in the zinc acetate solution and was analysed according to Cline (1969).

#### 261 **Total organic carbon**

262 To quantify sediment TOC, samples collected in 2023 were dried under anoxic conditions, while those from  
263 2022 were dried under oxic conditions, at room temperature until constant weight was reached. Sediments from both  
264 years were milled and analysed by a TOC analyser (SoliTOC Cube Elementar, Germany).

#### 265 **2.6 Molecular biology analysis**

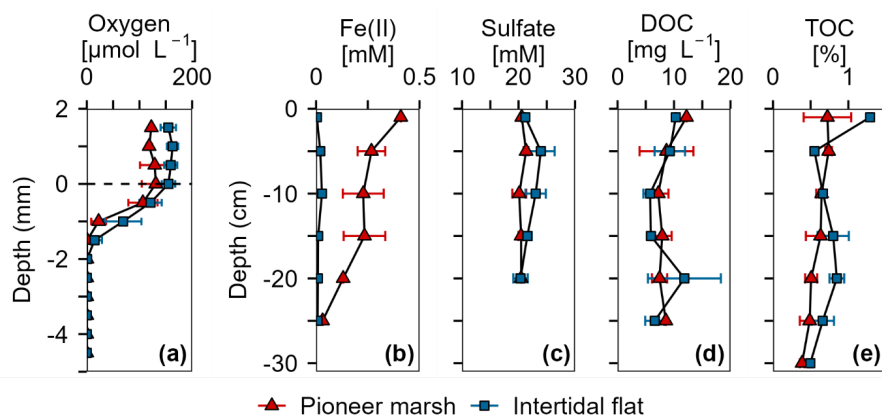
266 The co-extraction of DNA and RNA was performed according to Lueders et al. (2004). Quantitative  
267 polymerase chain reaction (qPCR) for DNA and complementary DNA (cDNA) was done to quantify total bacterial  
268 16S rRNA gene copies using the primer 341F and 797R. Functional genes were also targeted: *Geobacter* spp. (involved  
269 in Fe(III) reduction) using the primer Geo 577F and Geo 822R, and *dsrA* (involved in SO<sub>4</sub><sup>2-</sup> reduction) using the primer  
270 DSR\_1F and DSR\_1R. Quantitative polymerase chain reaction was done using SsoAdvanced SYBR Green Supermix  
271 (Bio-Rad) on the C1000 Touche Thermal Cycler (CFX96™ Real-Time System, Bio-Rad, Germany). Data analysis  
272 was performed by the software Bio-Rad CFX Maestro 1.1 (version 4.1.2433.1219). Further details are given in  
273 Supplement, S1.6 and Table S2.

274 **2.7 Statistical analysis**

275 For statistical analysis RStudio (R version R-4.4.3) was used (R Core Team, 2025). The significance level for  
276 all tests was set at  $p < 0.05$ . Normal distribution of the data and homogeneity of variances were tested by Shapiro-Wilk  
277 test and Levene test, respectively. Correlations between parameters was tested with the relevant tests (Pearson's  
278 correlation test or Spearman's rank correlation test depending on the normality of the data). Statistical differences  
279 between two groups were tested with a t-test and for more than two groups with a one-way Analysis of Variance  
280 (ANOVA) or Kruskal-Wallis rank sum test. For differences in the CO<sub>2</sub> release, a linear mixed model was applied.  
281 More details on the chosen tests and model are given in Supplement, S1.7. We reported the p-value in the text; further  
282 relevant statistical test results and parameters are shown in the corresponding sections in the SI. The variability of the  
283 geochemistry analysis is represented by the standard deviation of triplicates/duplicates. For the in situ experiment, the  
284 variability is reflected in the standard error of triplicates. For duplicate analyses, variability reflects the range of the  
285 two samples.

286 **3 Results**

287 **3.1 Geochemistry at the study site**



288  
 289 **Figure 2. Overview of porewater and sediment biogeochemistry in terms of electron acceptors ( $\text{O}_2$ ,  $\text{Fe(III)}$ ,  $\text{SO}_4^{2-}$ ) and**  
 290 **electron donor (DOC, TOC) from in situ push cores in the pioneer marsh (red triangles) and intertidal flat (blue squares).**  
 291 (a) Oxygen concentration profiles measured in intact cores using microsensors. Note that these cores were collected in 2022, separate  
 292 from the push cores used for analysis shown in (b-e). Two cores were collected from each zone and two to four profiles were taken  
 293 from each core, shortly (within hours) after sampling. (b) Ferrous iron in the porewater, as an indicator of  $\text{Fe(III)}$  reduction. (c)  
 294 Sulfate concentrations in the porewater. (d) Dissolved organic carbon in the porewater. (e) Total organic carbon in the sediment.  
 295 For (b-d), push cores were taken in triplicates in both zones to a depth of 25 cm in 2023. Duplicate push cores for (e) the TOC were  
 296 sampled in 2022. For all sub-figures, markers denote mean  $\pm$  standard deviation (due to limited sample mass, some depth values  
 297 only show mean and the range of two samples, or only a single value). All cores were sampled during low tide.

298 Porewater and solid phase measurements from the push and microsensor cores analysis show availability of  
 299 electron acceptors ( $\text{O}_2$ ,  $\text{Fe(III)}$ , and  $\text{SO}_4^{2-}$ ) over depth in both the pioneer marsh and intertidal flat (Fig. 2). In the pioneer  
 300 marsh,  $\text{O}_2$  decreased from  $131.02 \pm 26.49 \mu\text{mol L}^{-1}$  at the sediment-water interface to  $0.18 \pm 0.12 \mu\text{mol L}^{-1}$  over 2 mm  
 301 and was depleted beyond this depth. We observed a similar trend for the intertidal flat, with  $155.17 \pm 12.71 \mu\text{mol L}^{-1}$   
 302 at the sediment-water interface, and a decrease to  $0.62 \pm 1.10 \mu\text{mol L}^{-1}$  at 2 mm depth before it was fully depleted (Fig.  
 303 2a). Aqueous  $\text{Fe(II)}$  (as an indicator of  $\text{Fe(III)}$  reduction) showed a decreasing trend in both zones, with higher  
 304 concentration in the pioneer marsh of  $267.49 \pm 66.77 \mu\text{M}$  at 5 cm depth and  $31.41 \mu\text{M}$  at 25 cm, and  $19.93 \pm 16.15$   
 305  $\mu\text{M}$  at 5 cm decreasing to  $7.20 \pm 2.89 \mu\text{M}$  at 25 cm in the intertidal flat (Fig. 2b). Sulfate was detected in the porewater  
 306 at all sampled depths (1.5 to 20 cm) in both zones (Fig. 2c). In the pioneer marsh, it ranged in the upper 20 cm from a  
 307 minimum of  $20.12 \pm 1.23$  to a maximum of  $21.34 \pm 0.43 \text{ mM}$  and in the intertidal flat from  $20.35 \pm 1.27$  to  $23.95 \pm$   
 308  $2.44 \text{ mM}$ . We observed a slight decrease in  $\text{SO}_4^{2-}$  concentration over depth which was more pronounced in the intertidal  
 309 flat. This is further supported by the ratio of sulfate:chloride (Fig. S2a). The ratio remained constant in the pioneer  
 310 marsh, while a slight decrease was measured in the intertidal flat. We also measured  $\text{SO}_4^{2-}$  at lower depths (up to 50

311 cm) in cores taken in 2022 and observed similar  $\text{SO}_4^{2-}$  concentrations (Fig. S2b). To complement the porewater Fe(II),  
312 we measured the 0.5 M HCl extractable Fe(III) from the bulk sediment from a depth up to 15-20 cm:  $1.30 \pm 1.08 \mu\text{mol}$   
313 Fe(III)  $\text{g}^{-1}$  dry sediment in the pioneer marsh and  $1.00 \pm 0.51 \mu\text{mol}$  Fe(III)  $\text{g}^{-1}$  dry sediment in the intertidal flat. The  
314 resulting Fe(II) to total iron ratio was  $0.98 \pm 0.02$  and  $0.98 \pm 0.01$  respectively.

315 Organic carbon as the likely electron donor was measured in the porewater as non-purgeable organic carbon  
316 and in the sediment as TOC. The DOC and TOC decreased slightly over depth (Fig. 2d/e) in both zones. In the pioneer  
317 marsh, the DOC was  $12.21 \text{ mg C L}^{-1}$  at the top (1 cm deep) and decreased over depth to  $8.55 \text{ mg C L}^{-1}$  at 25 cm. For  
318 the intertidal flat, the DOC at the top (1 cm deep) was  $10.31 \text{ mg C L}^{-1}$  and decreased to  $6.60 \pm 1.69 \text{ mg C L}^{-1}$  at 25 cm.  
319 The TOC decreased from  $0.7 \pm 0.3 \%$  at the top to  $0.5 \pm 0.1 \%$  at a depth of 25 cm in the pioneer marsh and from  $1.3 \%$   
320 to  $0.7 \pm 0.2 \%$  in the intertidal flat (Fig. 2e). Concentrations at lower depths are shown in Supplement, Fig. S2c, and  
321 are in a similar range. In both the pioneer marsh and intertidal flat, no  $\text{CH}_4$  release, neither as fluxes or in the porewater  
322 up to a depth of 50 cm, was detected (detection limit: 0.28 and 0.53 ppm respectively; Table S3).

323 Particle size analysis indicated that sediment from the pioneer marsh was dominated by fine particles, whereas  
324 the intertidal flat sediment was coarser. In the sediment of the pioneer marsh, we determined  $41.7 \pm 9.1 \%$  sand,  
325  $38.7 \pm 2.5 \%$  silt, and  $19.7 \pm 8.1 \%$  clay. For the sediment of the intertidal flat, a higher sand fraction ( $61.5 \pm 0.5 \%$ ),  
326 less silt ( $29.0 \pm 5.0 \%$ ), and notably lower clay content ( $9.5 \pm 5.5 \%$ ) was measured. For more details on the size  
327 fractions, see Supplement, Table S4.

## 328 **3.2 In situ organic carbon manipulation experiment**

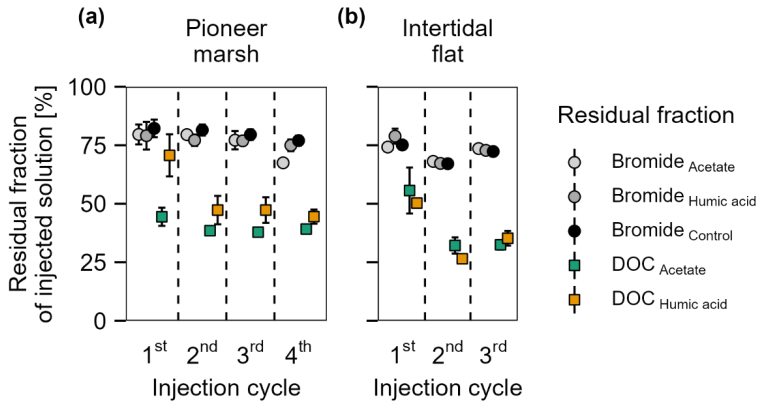
### 329 **3.2.1 Distribution of bromide tracer and dissolved organic carbon in the sediment**

330 Bromide was used in the in situ experiment as an inert tracer to test the washing out of the injection solution  
331 from the experimental plot over the sampling time of one injection cycle (48 h). The native  $\text{Br}^-$  concentration was  
332  $0.66 \pm 0.02 \text{ mM}$  in the pioneer marsh and  $0.63 \pm 0.01 \text{ mM}$  in the intertidal flat. Assuming an equal distribution of the  
333 injected solution in the experimental cylinder, we expected the  $\text{Br}^-$  concentration to increase by  $0.30 \text{ mM}$  to a final  
334 concentration of  $0.99 \text{ mM}$  in the plots of the pioneer marsh and by  $0.32 \text{ mM}$  to a final concentration of  $0.97 \text{ mM}$  for  
335 the plots in the intertidal flat (calculations Supplement, S1.4 – expected  $\text{Br}^-$  concentration). Throughout a test injection  
336 cycle with the same sampling intervals as the experimental injection cycles, the  $\text{Br}^-$  concentration remained above the  
337 background level with a gradual decrease over time in both zones (Figs. S3a/b). Overall, after 48 h (one injection  
338 cycle),  $\text{Br}^-$  levels in the porewater remained elevated in each cycle for both zones. In the pioneer marsh, an average of  
339  $77.5 \pm 5.9 \%$  of the expected level of  $\text{Br}^-$  remained in the porewater of the experimental cylinder. The intertidal flat  
340 had a slightly lower average residual fraction of  $72.1 \pm 4.4 \%$  of the expected  $\text{Br}^-$  level across all injection cycles (Fig.  
341 3). Here, residual fraction is defined as the ratio between the  $\text{Br}^-$  concentration measured in the porewater 48 h post  
342 injection and the expected total  $\text{Br}^-$  concentration in an experimental cylinder (Eq. (1); details in S1.4). The expected  
343 total  $\text{Br}^-$  concentration includes both the native  $\text{Br}^-$  and the added  $\text{Br}^-$  during the experiment (expected  $\text{Br}^-$ ) after  
344 accounting for dilution in the sediment. Details on the calculation of the  $\text{Br}^-$  residual fraction are provided in  
345 Supplement, S1.4.

346

$$\frac{\text{Br}^- \text{ concentration at the end of an injection cycle}}{\text{Br}^- \text{ expected}} = \text{residual fraction} \quad (1)$$

347 The residual fraction of DOC is defined in the same way as for Br<sup>-</sup>, representing the proportion of measured  
348 DOC after 48 h to the expected DOC (native DOC + added acetate/humic acid) and was calculated analogously to Br<sup>-</sup>  
349 , with DOC concentrations used instead (Eq. (1) and S1.4). Comparing the average residual fraction of DOC and Br<sup>-</sup>  
350 (Fig. 3) across all injection cycles, the DOC fraction was significantly lower in both the pioneer marsh and intertidal  
351 flat (Br<sup>-</sup> vs. acetate and Br<sup>-</sup> vs. humic acid) ( $p \leq 0.001$ , Table S5). In the pioneer marsh,  $40.0 \pm 1.2$  % of the injected  
352 DOC in the acetate treatment remained, on average across all injection cycles, while the corresponding value for the  
353 humic acid treatment was  $52.9 \pm 4.5$  %. In the intertidal flat, relatively less carbon remained, with a smaller difference  
354 between the carbon sources. Here, the mean residual fraction was  $38.2 \pm 4.8$  % for the acetate treatment and  $37.3 \pm 3.6$   
355 % for the humic acid treatment.

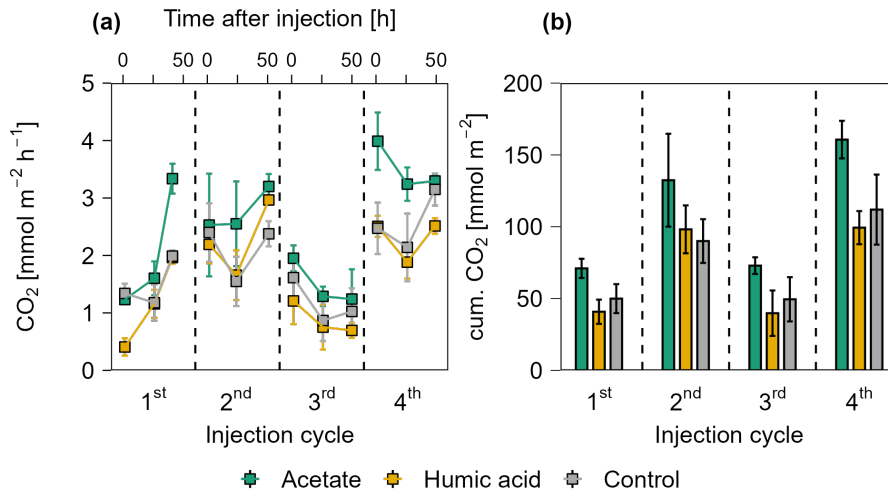


356

357 **Figure 3. Residual fraction of injected solutions (Br<sup>-</sup> and DOC) in percentage after 48 h for treatments (acetate, humic acid)**  
358 **and control plots in the (a) pioneer zone (over four injection cycles) and (b) intertidal flat (over three injection cycles).**  
359 Coloured squares show the residual fraction of injected DOC (acetate in green and humic acid in orange). The grey shaded circles  
360 represent the residual of Br<sup>-</sup> from the different treatments and the control. The values were calculated based on the ratio between  
361 the measured DOC or Br<sup>-</sup> concentration (porewater concentration 48 h post injection) and the expected DOC or Br<sup>-</sup> concentration  
362 (native + added). Markers represent the mean of the triplicates, with error bars indicating the corresponding standard error for  
363 treatments and control in both zones for DOC and Br<sup>-</sup> across all injection cycles.

364 3.2.2 Effect of organic carbon input in the pioneer marsh

365 Carbon dioxide release



366

367 **Figure 4.** CO<sub>2</sub> release over four OC injection cycles for the acetate, humic acid, and control plots in the pioneer marsh. The  
368 dashed lines separate the individual injection cycles. (a) presents individual measured CO<sub>2</sub> fluxes 1.5, 24, and 48 h after injection  
369 in CO<sub>2</sub> mmol m<sup>-2</sup> h<sup>-1</sup>. Acetate (green), humic acid (orange), and NaCl for the control (grey) were injected into the sediment and  
370 GHG fluxes were measured directly above the injection spot at the aforementioned time intervals. (b) shows the cumulative CO<sub>2</sub>  
371 emissions in CO<sub>2</sub> mmol m<sup>-2</sup> over one injection cycle for each treatment and control. We note here that some variability in the fluxes  
372 based on factors such as day/night could not be captured in our sampling approach; we therefore aimed to use a consistent approach  
373 and report relative changes rather than emphasize absolute values. For (a/b), markers represent mean ± standard error of triplicates  
374 for all treatments and the control across injection cycles. For the 1<sup>st</sup> and 3<sup>rd</sup> injection cycle for the acetate treatment (both 1.5 h  
375 values) were based on duplicate measurements, which is thus also the case for the (b) cumulative CO<sub>2</sub> emission of these cycles.

376 **Figure 4** presents the CO<sub>2</sub> release for each injection cycle with the individual CO<sub>2</sub> fluxes 1.5, 24, and 48 h  
377 post injection (Fig. 4a) and the cumulative CO<sub>2</sub> emissions (Fig. 4b) in the pioneer marsh. For all four injection cycles,  
378 the CO<sub>2</sub> fluxes of the acetate treated plots exceeded the CO<sub>2</sub> fluxes of the humic acid and control plots (Fig. 4a). For  
379 the first injection cycle, the acetate treatment was significantly higher compared to the humic acid treatment ( $p < 0.05$ ,  
380 Table S6) and slightly above the threshold for statistical significance ( $p = 0.08$ , Table S6) compared to the control. In  
381 the following injection cycle, the CO<sub>2</sub> fluxes of the acetate treatment were also higher compared to the humic acid and  
382 control plots but not significantly ( $p > 0.05$ ). Hence, the acetate treated plot consistently exhibited the highest fluxes.  
383 The difference between the humic acid and control plots was statistically negligible ( $p > 0.05$ ). Similarly, the  
384 cumulative CO<sub>2</sub> emissions from the acetate treated plots were the highest while the emissions from the humic acid and

Deleted: Figure 4  
Formatted: Font: 10 pt, Not Bold  
Formatted: Font: 10 pt, Not Bold, Not Italic, Check spelling and grammar

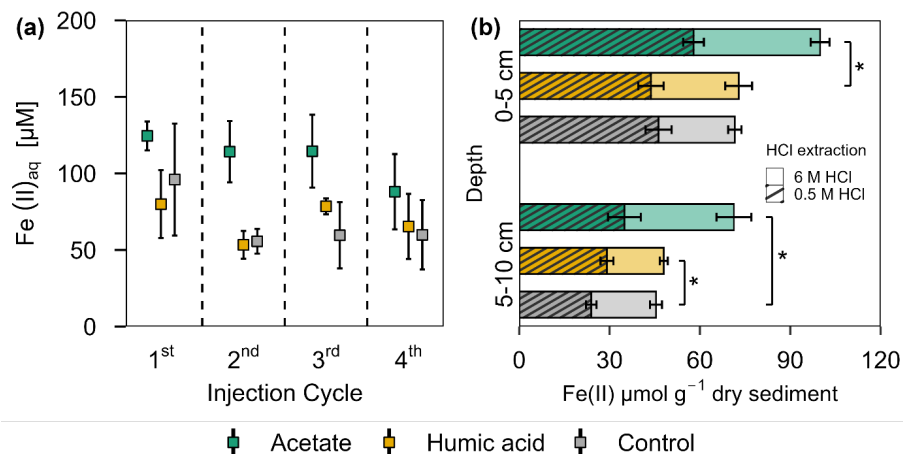
386 control plots were in a similar range for all four injection cycles (Fig. 4b). The CO<sub>2</sub> emitted from the acetate treated  
387 plots was up to  $83.2 \pm 53.7$  % higher than for the humic acid treated plots. Similarly, the emissions of the acetate plots  
388 were up to  $47.4 \pm 36.4$  % higher relative to the control plots. No statistical differences were measured between the  
389 cumulative CO<sub>2</sub> emission of the acetate treated plots and the control or humic acid treatment. Overall, these differences  
390 were smaller than those seen at individual CO<sub>2</sub> fluxes at specific time points (Fig. 4a), likely due to high variability in  
391 fluxes that resulted in variable cumulative CO<sub>2</sub> emissions. In all treatments and the control, no CH<sub>4</sub> as a flux was  
392 detected (lower than detection limit (0.28 ppm); Table S3).

393 The CO<sub>2</sub> fluxes showed a positive correlation with air temperature and a moderate positive correlation with  
394 the tidal cycle in the pioneer marsh (Table S7). Specifically, CO<sub>2</sub> fluxes were found to be higher as the spring tide  
395 receded. Lower CO<sub>2</sub> fluxes were measured during the first and third injection cycles, which occurred close to spring  
396 tides.

397 Further differences between the treatments and control were observed in the DOC concentrations (Fig. S4)  
398 and the residual fraction of DOC (Fig. 3a) in the pioneer marsh. Over all four injection cycles, the average DOC  
399 concentration in the acetate treated plots did not significantly differ from the control ( $p > 0.05$ ), while the DOC  
400 concentrations of the humic acid treated plots were significantly higher than the concentrations of acetate treated plots  
401 and the control plots ( $p < 0.05$ , Table S8). These differences are consistent with the residual fraction of DOC (Fig. 3a).  
402 Across all four injection cycles, the average residual fraction in the humic acid treatment was significantly higher  
403 compared to the acetate treatment but significantly lower than the Br<sup>-</sup> residual fraction ( $p < 0.002$ ,  $p < 0.001$   
404 respectively, Table S5). No difference in the TOC content was found between treatments and control in both depths.  
405 The content ranged from  $0.9 \pm 0.1$  % to  $1.2 \pm 0.1$  % in the upper 5 cm, with a slight decrease at lower depth (Table S9).

406 In addition to the gas fluxes, we also measured DIC and pH of the porewater for each treatment and control  
407 for each injection cycle (Fig. S5). As the differences in the CO<sub>2</sub> fluxes were more pronounced and our focus was on  
408 GHG release, we only present and later discuss these data.

409 Effect of organic carbon input on the geochemistry of porewater and sediment



410  
 411 **Figure 5. Ferrous iron in (a) porewater and (b) solid phase from acetate and humic acid treated plots and the control plots**  
 412 **in the pioneer marsh.** (a) Aqueous ferrous iron (Fe(II)<sub>aq</sub>) [µM] sampled after each injection cycle (cycles are separated by the  
 413 dashed line). Triplicates for each treatment and control for each injection cycle were collected and mean ± standard error is shown.  
 414 (b) HCl extractable Fe(II) content [µmol g<sup>-1</sup> dry sediment] at two different depths (0-5 and 5-10 cm) sampled at the end of all four  
 415 injection cycles. Different colour coding was used for contrasting treatments: acetate treatment (green), humic acid treatment  
 416 (orange), and control (grey). Striped bars represent poorly crystalline Fe(II) (0.5 M HCl extraction) and solid bars higher crystalline  
 417 Fe(II) (6 M HCl extraction). The 0.5 M HCl extract was subtracted from the 6 M HCl extracted fraction to separate poorly and  
 418 higher crystalline Fe(II). Significance is denoted for the 0.5 M HCl extraction. Statistical details are given in the SI (Table S11),  
 419 significance level  $p < 0.05$  \*. For each treatment and control, each spatial triplicate ( $n = 3$ ) was analyzed in triplicate (total  $n = 9$ )  
 420 for each depth (0-5 and 5-10 cm); results are presented as mean ± standard error.

421 In the pioneer marsh, acetate treated plots had significantly higher aqueous Fe(II) concentrations compared  
 422 to humic acid and control plots when considering the average concentration across all injection cycles (acetate vs.  
 423 humic acid  $p = 0.007$  and vs. control  $p = 0.002$ , Table S10). Although the differences were not always statistically  
 424 significant for the individual cycles, the Fe(II) concentration in the porewater of the acetate treated plots was  
 425 consistently higher (Fig. 5a): 1<sup>st</sup> cycle  $124.52 \pm 9.44$  µM, 2<sup>nd</sup> cycle  $114.20 \pm 19.98$  µM, 3<sup>rd</sup> cycle  $114.54 \pm 23.80$  µM,  
 426 and 4<sup>th</sup> cycle  $88.08 \pm 24.58$  µM. Humic acid treated plots and the control plots showed similar aqueous Fe(II)  
 427 concentrations. For humic acid treated plots the aqueous Fe(II) concentration ranged between  $53.36 \pm 9.05$  µM  
 428 (2<sup>nd</sup> cycle) and  $79.96 \pm 22.16$  µM (1<sup>st</sup> cycle), and for the control between  $55.69 \pm 8.04$  (2<sup>nd</sup> cycle) and  $96.01 \pm 36.61$   
 429 µM (1<sup>st</sup> cycle) (Fig. 5a).

430 A similar trend can be seen in the solid phase for the HCl extractable Fe(II), for both extractions approaches  
 431 (0.5 M and 6 M HCl) (Fig. 5b). Comparing the poorly crystalline Fe(II) fraction, the acetate treatment had the highest

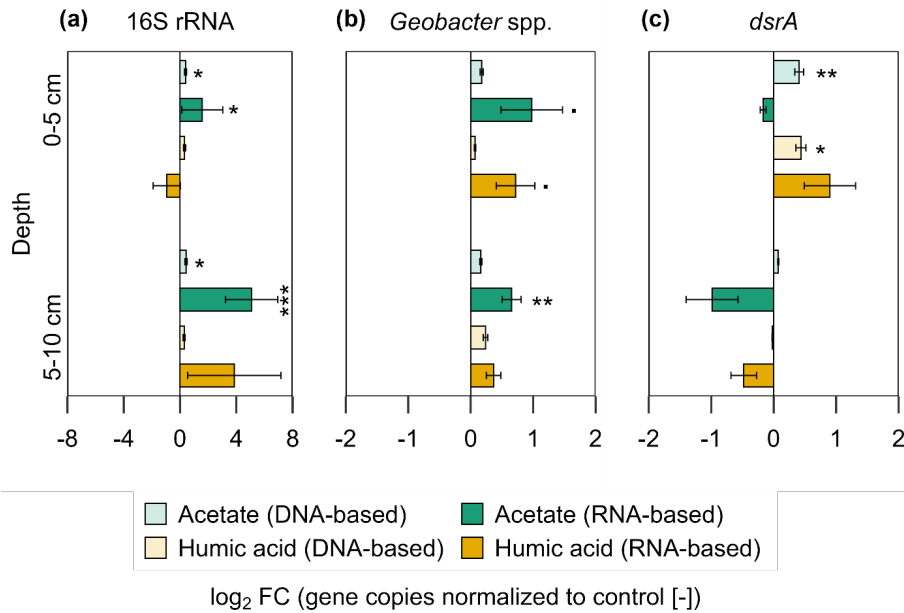
432 Fe(II) content compared to the humic acid treatment and the control at both depths. Acetate treated plots showed an  
433 Fe(II) content of  $57.87 \pm 3.44 \mu\text{mol g}^{-1}$  sediment in the upper 5 cm and  $34.91 \pm 5.45 \mu\text{mol g}^{-1}$  sediment from 5-10 cm.  
434 Humic acid and control plots had similar levels of Fe(II): for the humic acid plots, the content in the upper 5 cm was  
435  $43.74 \pm 4.18 \mu\text{mol g}^{-1}$  sediment and from 5-10 cm, it was  $29.13 \pm 2.12 \mu\text{mol g}^{-1}$  sediment. The control plots showed  
436  $46.28 \pm 4.32 \mu\text{mol g}^{-1}$  sediment in the upper 5 cm and  $23.93 \pm 1.75 \mu\text{mol g}^{-1}$  sediment between 5 to 10 cm. We observed  
437 the same trend for the higher crystalline Fe(II) content. The acetate treatment had the highest contents with  $42.04 \pm 3.12$   
438  $\mu\text{mol g}^{-1}$  sediment (0-5 cm) and  $36.38 \pm 5.79 \mu\text{mol g}^{-1}$  sediment compared with humic acid or control plots. For both  
439 depth and crystallinities, the acetate treatment showed significantly the highest content, in nearly all comparisons to  
440 the humic acid or control plots (Table S11). Except for poorly crystalline Fe(II) at 5-10 cm depth, humic acid and  
441 control plots did not differ significantly (Table S11).

442 No consistent difference was detected in  $S(\text{II})_{\text{tot}}$  in the porewater of the pioneer marsh (Fig. S6a). The  $S(\text{II})_{\text{tot}}$   
443 concentrations were in the same range: acetate from  $3.16 \pm 0.01 \mu\text{M}$  (4<sup>th</sup> cycle) to  $5.59 \pm 1.21 \mu\text{M}$  (1<sup>st</sup> cycle), humic  
444 acid from  $3.0 \pm 0.11 \mu\text{M}$  (4<sup>th</sup> cycle) to  $6.34 \pm 1.56 \mu\text{M}$  (1<sup>st</sup> cycle) and control from  $3.63 \pm 0.34 \mu\text{M}$  (1<sup>st</sup> cycle) to  
445  $4.39 \pm 1.13 \mu\text{M}$  (4<sup>th</sup> cycle). Also, statistical analysis did not reveal a difference between the different treatments and  
446 control  $S(\text{II})_{\text{tot}}$  averaged over all cycles ( $p > 0.05$ ). Similarly, AVS measurements of the solid sulfide species showed  
447 no difference between treatments and the control (Fig. S6b). In the upper 5 cm, contents were similar (acetate:  
448  $6.13 \pm 1.40$ , humic acid  $3.89 \pm 1.19$ , and control  $7.37 \pm 1.76 \mu\text{mol g}^{-1}$  sediment). Similar contents were measured at  
449 5-10 cm depth, with no coherent trend between the layers.

#### 450 **Effect of organic carbon input on microbial growth and metabolic activity**

451 The impact of the added OC on the bacterial community was analysed by qPCR. The analyses were based on  
452 DNA (microbial abundance) and RNA (metabolically active microorganisms). The results show the gene copies of  
453 both treatments normalized to the control as  $\log_2$  fold change ( $\log_2 \text{FC}$ ) (Fig. 6). Statistics are based on the absolute  
454 gene copy numbers (Fig. S7). For the acetate treated plots a significantly higher bacterial 16S rRNA gene copy number  
455 (DNA- and RNA-based) was measured compared to the control plots across all analysed depths (Fig. 6a;  $p < 0.05$ ). In  
456 comparison to the control, DNA-based bacterial 16S rRNA gene copies increased by a factor of  $0.4 \pm 0.07$  ( $\log_2 \text{FC}$ )  
457 under acetate treatment and their potential activity, indicated by RNA, increased by  $1.58 \pm 1.46 \log_2 \text{FC}$  in the upper 5  
458 cm. This remained similar at the depth of 5-10 cm, with an increase in DNA-based 16S rRNA gene copies by  $0.43 \pm$   
459  $0.09 \log_2 \text{FC}$  and an increase in activity (RNA) by  $5.09 \pm 1.86 \log_2 \text{FC}$ . For the comparison between plots amended  
460 with humic acid and the control, variations were observed but no significant differences were measured ( $p > 0.05$ ).  
461 Microbial activity (RNA) of *Geobacter* spp., were higher in the acetate and humic acid treatment compared to the  
462 control in the upper 5 cm, however, slightly over the significance criterion (Fig. 6b;  $p = 0.051$ ,  $p = 0.057$ , respectively).  
463 For the acetate treated plots, the activity (RNA-based) of *Geobacter* spp. was higher compared to the control by a  
464 factor of  $0.98 \pm 0.49$ . The humic acid treatment also had upregulated activity by a factor of  $0.72 \pm 0.31$ . The higher  
465 microbial activity of *Geobacter* spp. remained significantly enhanced ( $p = 0.008$ ) for the acetate treatment compared  
466 to the control at the lower depth (RNA-based:  $\log_2 \text{FC}$ :  $0.66 \pm 0.15$ ), too. The addition of OC did not affect the microbial  
467 activity (RNA) of *dsrA* genes at both depths (Fig. 6c) in the pioneer marsh. However, the abundance (DNA) of *dsrA*

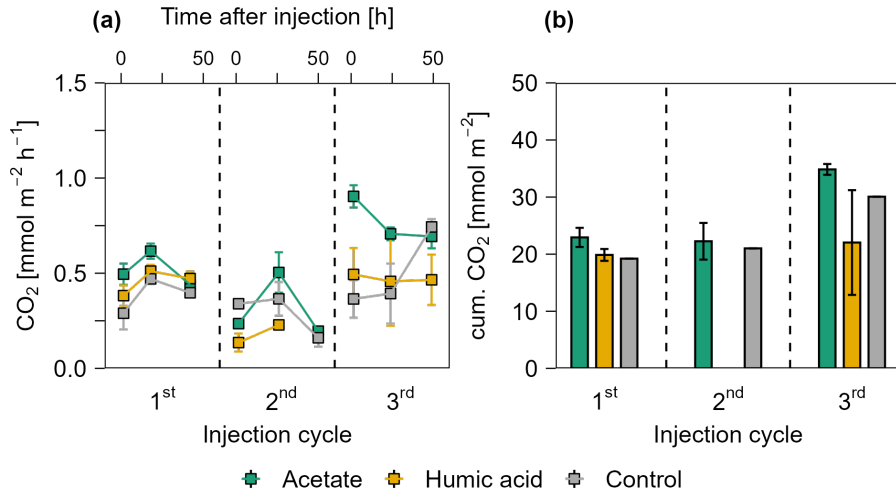
468 genes in the upper layer was significantly higher for both treatments (acetate  $p = 0.006$ , humic acid  $p = 0.015$ ). Absolute  
 469 gene copy numbers are given in Supplement, Fig. S7 and statistical details in Table S12.



470  
 471 **Figure 6. Bacterial gene copy numbers of (a) 16S rRNA (16S), (b) *Geobacter* spp., and (c) *dsrA* for acetate and humic acid**  
 472 **treatment normalized to the control in the pioneer marsh.** The values are represented as  $\log_2$  fold change (FC). Values > 0  
 473 indicate an upregulation while values < 0 indicate downregulation of the genes compared to the control (acetate in green, humic  
 474 acid in orange). DNA-based numbers are given in lighter colours and RNA-based in darker colours. Statistical differences in the  
 475 absolute gene copy numbers are indicated as stars in the figure: significant codes are  $p = 0.05$ .,  $p \leq 0.05$  \*,  $p \leq 0.01$  \*\*, and  
 476  $p \leq 0.001$  \*\*\*. Absolute gene copy numbers given in Supplement, Fig. S7. Sample sizes include triplicates of each treatment and  
 477 control at both depths, represented as mean  $\pm$  standard error (exception of duplicate measurements for 16s RNA-based humic  
 478 substances (5-10 cm) and 16s RNA-based control (0-5 cm)).

479 3.2.3 Effect of organic carbon input in the intertidal flat

480 Carbon dioxide release



481

482 **Figure 7.** CO<sub>2</sub> release over three injection cycles for the acetate and humic acid treated plots and the control plots in the  
 483 intertidal flat. (a) CO<sub>2</sub> fluxes after 1.5, 24, and 48 h after injection in CO<sub>2</sub> mmol m<sup>-2</sup> h<sup>-1</sup> over three injection cycles. The dashed  
 484 lines separate the individual injection cycles. In the 2<sup>nd</sup> injection cycle, fluxes in the humic acid treatment are only displayed at 1.5  
 485 and 24 h post injection due to missing data. Acetate (green), humic acid (orange), and NaCl for the control (grey) were injected into  
 486 the sediment and GHG fluxes were measured directly above the injection spot at the aforementioned time intervals. (b) presents the  
 487 cumulative CO<sub>2</sub> release in mmol CO<sub>2</sub> m<sup>-2</sup> over one injection cycle for each treatment and control. Due to missing values for humic  
 488 acid amended plots in the second injection cycle, cumulative emissions could not be calculated. For the same reason, standard errors  
 489 of the control plots are also not available. For (a/b), markers represent the mean ± standard error of triplicates for all treatments and  
 490 the control across injection cycles, except where missing values for CO<sub>2</sub> release occurred due to nonlinear CO<sub>2</sub> release during the  
 491 gas sampling incubation time. (a) duplicate measurements are reflected for the 1<sup>st</sup> injection cycle for the control (1.5 and 24 h), for  
 492 the 2<sup>nd</sup> injection cycle for the acetate treatment and control (48 h), and the 3<sup>rd</sup> injection cycle for the acetate treatment and control  
 493 (1.5, 24, and 48 h). Single measurement values are shown for the control in the 1<sup>st</sup> (48 h) and 2<sup>nd</sup> (1.5 h) injection cycle. For (b),  
 494 cumulative CO<sub>2</sub> emissions, the acetate treatment shows duplicate measurements for the 2<sup>nd</sup> and 3<sup>rd</sup> injection and for the control,  
 495 only single values are reflected.

496 **Figure 7a** presents the CO<sub>2</sub> release from the intertidal flat over three injection cycles 1.5, 24, and 48 h post  
 497 injection. Acetate treated plots released the highest CO<sub>2</sub> in all three injection cycles compared to the humic acid and  
 498 the control plots. Similar to the pioneer marsh, no strong differences were observed between humic acid treated plots  
 499 and the control plots. Consistently, the maximum cumulative CO<sub>2</sub> emissions were observed in the acetate treated plots  
 500 (Fig. 7b). Due to nonlinearity of CO<sub>2</sub> release over the incubation time of gas sampling, some data points are missing;

**Deleted:** Figure 7

**Formatted:** Font: 10 pt, Not Bold

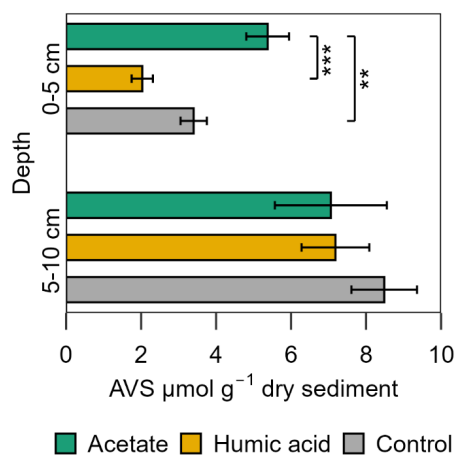
**Formatted:** Font: 10 pt, Not Bold, Not Italic, Check spelling and grammar

502 therefore, statistical comparison of CO<sub>2</sub> release between treatments and the control was not done. Nevertheless, plots  
503 amended with acetate consistently showed higher CO<sub>2</sub> releases across all injection cycles. Methane was not detected  
504 in the fluxes of any treatment in the intertidal flat plots (lower than detection limit (0.28 ppm); Table S3). Similar to  
505 the pioneer marsh, we focus here on CO<sub>2</sub> data although DIC and pH were measured (Fig. S8).

506 No difference in the DOC concentrations between the treatments and the control were measured (Fig. S9).  
507 Similarly, no difference was measured between the residual fraction (recovery of injected DOC) between acetate and  
508 humic acid treatments (Fig. 3b). The TOC content among the treatments and the control was also in the same range  
509 (0.4-0.5 %) (Table S9).

#### 510 Effect of organic carbon input on the geochemistry of porewater and sediment

511 In the intertidal flat, aqueous Fe(II) concentrations ranged from  $9.25 \pm 0.21$  to  $24.82 \pm 4.50$   $\mu\text{M}$  in both  
512 treatments and the control, with no significant differences ( $p > 0.05$ ) (Fig. S10a). Additionally, no difference between  
513 the treatments and the control was detected in the solid phase for both crystallinities (0.5 and 6 M HCl extraction) and  
514 depths. In the upper 5 cm, the content of the poorly crystalline Fe(II) ranged from  $18.28 \pm 1.28$  to  $19.60 \pm 0.88$   $\mu\text{mol g}^{-1}$   
515 sediment among all treatments and control, while in the deeper layer, the range was from  $18.11 \pm 0.71$  to  $24.59 \pm 1.22$   
516  $\mu\text{mol g}^{-1}$  sediment. The content of the higher crystalline Fe(II) ranged from  $11.68 \pm 0.99$  to  $20.06 \pm 3.64$   $\mu\text{mol g}^{-1}$   
517 sediment in the upper 5 cm and from  $12.98 \pm 1.03$  to  $17.50 \pm 2.75$   $\mu\text{mol g}^{-1}$  sediment at a depth of 5-10 cm (Fig. S10b).



518  
519 **Figure 8. Acid volatile sulfide (AVS) in the solid phase sampled at the end of the experiment for the acetate and humic acid**  
520 **treated plots and the control plots in the intertidal flat.** AVS [ $\mu\text{mol g}^{-1}$  dry sediment] content of the solid phase from the different  
521 treatments (acetate in green, humic acid in orange) and control (grey). Significance is denoted for the upper sediment layer (0-5  
522 cm), deeper layer no statistically significant difference occurred. Statistical details are given in the SI (Table S13), significance level

523  $p < 0.05$  \*,  $p < 0.01$  \*\*, and  $p < 0.001$  \*\*\*. Each spatial triplicate ( $n=3$ ) was analyzed in triplicates (total  $n = 9$ ) for each treatment  
524 and the control at both depths; results are presented as mean  $\pm$  standard error.

525 For porewater  $S(II)_{tot}$ , no large differences were measured between the treatments and control in the intertidal  
526 flat. The concentrations of both treatments and the control were in a similar range over all injection cycles,  $0.62 \pm 0.01$   
527 to  $1.73 \pm 0.67 \mu\text{M } S(II)_{tot}$  (Fig. S11). In contrast, the AVS in the solid phase exhibited a significant difference between  
528 the treatments and the control (Fig. 8). Higher AVS contents were measured in the acetate plots. This difference was  
529 strongly pronounced in the upper 5 cm in the acetate plots relative to the setups amended with humic acid and the  
530 control ( $p < 0.001$  and  $p = 0.007$ , respectively, Table S13). AVS content in the upper 5 cm was  $5.38 \pm 0.57 \mu\text{mol g}^{-1}$   
531 sediment from the acetate plots,  $2.03 \pm 0.28 \mu\text{mol g}^{-1}$  sediment from the humic acid plots, and  $3.40 \pm 0.35 \mu\text{mol g}^{-1}$   
532 sediment from the control. In the deeper layer (5-10 cm), the differences between treatments and control were  
533 statistically negligible ( $p > 0.05$ ).

#### 534 **Effect of organic carbon input on microbial growth and metabolic activity**

535 In the intertidal flat, an increase in DNA- and RNA-based gene copy numbers of the bacterial 16S rRNA gene  
536 was detected in the acetate treatment compared to the control at both depths (0-5 and 5-10 cm) (Fig. S12a). This  
537 increase was significant for DNA and RNA in the upper layer and remained significant for RNA in the lower layer ( $p$   
538 = 0.008,  $p = 0.01$ , and  $p = 0.008$ , respectively). The acetate treatment showed a  $3.62 \pm 2.41 \log_2$  FC increase in the  
539 metabolic activity (RNA) of the total microbial community compared to the control in the upper layer and an increase  
540 of  $2.73 \pm 1.41 \log_2$  FC from 5-10 cm. For *Geobacter* spp. (Fig. S12b) the RNA-based gene copies were significantly  
541 higher compared to the control ( $p < 0.001$ ) by a factor of  $0.6 \pm 0.10$  in the upper 5 cm. No significant increase in the  
542 RNA-based copy numbers of *dsrA* genes in both depths (Fig. S12c) were observed; however, we detected slightly  
543 higher RNA-based *dsrA* gene copies in the acetate treatments ( $0.33 \pm 0.06 \log_2$  FC) compared to the control in the  
544 upper layer. Absolute gene copy numbers are presented in Fig. S13 and statistical details in Table S14.

## 545 4 Discussion

### 546 4.1 Geochemistry at the study site

547 Porewater and solid phase measurements from the push cores showed availability of electron acceptors ( $O_2$ ,  
548  $Fe(III)$ , and  $SO_4^{2-}$ ) at different depths in both the pioneer marsh and intertidal flat. Based on microsensor measurements  
549 during low tide, we observed  $O_2$  concentrations in the top 2 mm decreasing with depth, from  $131.02 \pm 26.49$  to  $0.18 \pm$   
550  $0.12 \mu\text{mol L}^{-1}$  in the pioneer marsh, and in the intertidal flat from  $155.17 \pm 12.71$  to  $0.62 \pm 1.10 \mu\text{mol L}^{-1}$ , reaching 0  
551  $\mu\text{M}$  below that depth. This finding directly affects which biogeochemical processes occur below this depth. Other  
552 studies conducted in comparable ecosystems have indicated that during high tide and/or daytime,  $O_2$  penetrates deeper  
553 into the sediment (de Beer et al., 2005; Bosselmann et al., 2003), but reducing conditions may prevail underneath and  
554 that the depth of  $O_2$  penetration might be influenced by sediment grain size. Both zones in our study showed a high  
555 proportion of fine particles (silt:  $29.0 \pm 5.0$  to  $38.7 \pm 2.5$  % and clay:  $9.5 \pm 5.5$  to  $19.7 \pm 8.1$  %). Such a size distribution  
556 retains more water (Novák and Hlaváčiková, 2019), resulting in water-filled pore spaces even during low tide, which  
557 limits gas exchange. We suggest that the lack of  $O_2$  penetration beyond 2 mm at our study site results from the presence  
558 of fine particles. Despite differences in the duration and magnitude of inundation between the zones, the depth of  $O_2$   
559 penetration remained similar, indicating that these factors do not influence  $O_2$  penetration depth and that reducing  
560 conditions prevail beyond the upper millimetres during both tidal conditions. We do not exclude that the presence of  
561 sparse vegetation in the pioneer marsh compared to no vegetation in the intertidal flat may cause differences in the  
562 intrusion of  $O_2$  into the sediment (Koop-Jakobsen et al., 2017; Maricle and Lee, 2002). However, we did not detect  
563 this difference in our  $O_2$  measurements. In addition to plants, benthic organisms such as worms may introduce  $O_2$  into  
564 the sediment and influence the biogeochemical cycling in the sediment (Huettel et al., 2014). As worms were present  
565 in both zones, it is likely that they play a role in  $O_2$  penetration and re-oxidizing of reduced  $Fe(II)$  or sulfide species  
566 (Figs. S14a-d). We expect that this effect is not substantially different for the two zones, as no large qualitative  
567 difference in the presence of worms was observed visually.

568 Below the oxic zone, alternative electron acceptors were present. We used  $Fe(II)$  porewater data as an  
569 indicator of  $Fe(III)$  reduction. A decrease in the aqueous  $Fe(II)$  from  $267.49 \pm 66.77$  to  $31.41 \mu\text{M Fe(II)}$  in the pioneer  
570 marsh and from  $19.93 \pm 16.15$  to  $7.20 \pm 2.89 \mu\text{M Fe(II)}$  in the intertidal flat was measured over 25 cm. Based on the  
571 presence of aqueous  $Fe(II)$ , we assumed that  $Fe(III)$  reduction is likely occurring in both zones, which is less  
572 pronounced in the intertidal flat. The observed decreasing trend over depth has been commonly seen in other studies  
573 of coastal sediment (Moeslund et al., 1994; Lowe et al., 2000). It suggests a depletion of bioavailable  $Fe(III)$  with depth  
574 and/or removal of aqueous  $Fe(II)$ . Aqueous  $Fe(II)$  can precipitate with sulfide, which forms through  $SO_4^{2-}$  reduction  
575 deeper in the sediment when more thermodynamically favourable electron acceptors are exhausted (Jørgensen et al.,  
576 2019). The  $Fe(II)$  porewater concentrations are in the range of other studies from salt marshes, especially for the pioneer  
577 marsh (0-800  $\mu\text{M}$ ) (Kostka et al., 2002b; Seyfferth et al., 2020). Concentrations of the intertidal flat are on the lower  
578 end of the studies mentioned above. Ferrous iron was the predominant iron species in the solid fraction extracted by  
579 0.5 M HCl in both zones. Manganese(IV) as an electron acceptor was not further considered as the total manganese  
580 concentration from the study site is  $5 \mu\text{mol g}^{-1}$  sediment (Kubeneck et al., 2025), and thus relatively low in comparison  
581 to the total iron concentration.

582 Sulfate has a major role in the oxidation of OC as an important electron acceptor in coastal wetlands due to  
 583 its frequent supply via the incoming seawater. We observed a slight decrease in  $\text{SO}_4^{2-}$  over a depth of 20 cm which  
 584 was more distinct in the intertidal flat, as seen in the sulfate to chloride ratio (Fig. S2a). This suggests some  $\text{SO}_4^{2-}$   
 585 reduction in the upper 20 cm. A similar pattern was observed at a comparable site where Fe(II) predominates over total  
 586 iron and porewater  $\text{SO}_4^{2-}$  concentration decreases with depth, albeit with slightly higher  $\text{SO}_4^{2-}$  concentrations (Kostka  
 587 et al., 2002b). The relatively high levels of  $\text{SO}_4^{2-}$  at all tested depths (>50 cm), supported the absence of detectable  
 588  $\text{CH}_4$  dissolved in the porewater or as an efflux. This is consistent with past studies such as Martens and Berner (1974)  
 589 who stated that if more than ~10 % of seawater  $\text{SO}_4^{2-}$  is still present,  $\text{CH}_4$  is not produced, as a thermodynamically  
 590 more favourable electron acceptor is available (Schlesinger and Bernhardt, 2013b). We examined different possible  
 591 explanations for the lack of detected  $\text{CH}_4$  as we could not entirely exclude that  $\text{CH}_4$  was produced further down in the  
 592 sediment and oxidized via anaerobic methane oxidation (AOM), as observed in some coastal wetlands (Capooci et al.,  
 593 2024; La et al., 2022; Wang et al., 2019), or by lateral transport to surrounding tidal channels (Trifunovic et al., 2020).  
 594 We did not measure any  $\text{CH}_4$  as an efflux or in the porewater over multiple field campaigns, similar to a study conducted  
 595 at the same study site by Kubeneck et al. (2025). We considered the sensitivity of detection: the detection limit for  
 596 porewater  $\text{CH}_4$  was 0.53 ppm (Table S3) which corresponds to 1.13  $\mu\text{mol/L}$  based on our sampling method. We would  
 597 expect that methane, if produced within the depths examined here, would be above this concentration as porewater  
 598 concentrations of  $\text{CH}_4$  in wetlands slightly inland within the Elbe estuary were much higher (0.16 to 2.46 mmol/L,  
 599 Kubeneck et al., 2025). It is possible that trace amounts of  $\text{CH}_4$  (ppb) were present below the detection limit. The few  
 600 other studies that have detected  $\text{CH}_4$  in the Wadden Sea were at depths where  $\text{SO}_4^{2-}$  was largely depleted (Røy et al.,  
 601 2008; Wu et al., 2015), which is not the case in our study. Furthermore, the absence of an observed decrease in  $\text{SO}_4^{2-}$   
 602 concentration, particularly in the pioneer marsh, suggest a lack of AOM until 50 cm, as  $\text{CH}_4$  and  $\text{SO}_4^{2-}$  are consumed  
 603 in a 1:1 stoichiometric ratio during sulfate AOM. Thus, our results indicate that  $\text{CH}_4$  production and consumption are  
 604 unlikely until 50 cm. Below these depths, these processes may be occurring. Further analysis of the microbial  
 605 community, and/or  $\text{CH}_4$  injection experiments would help to determine if methanogenesis and AOM occur at lower  
 606 depths. Based on the high concentrations of  $\text{SO}_4^{2-}$  with relatively low changes with depth as well as the lack of  
 607 detectable  $\text{CH}_4$ , we suggest that electron acceptors may not be limiting the microbial turnover of OC and release of  
 608  $\text{CO}_2$  in our study. To our knowledge, this is rarely reported for coastal wetlands and not commonly expected for  
 609 terrestrial ecosystems. Here, we caution that further measurements of rates of electron acceptor turnover and/or  
 610 incubation experiments are needed to unambiguously exclude an electron acceptor limitation.

611 We also considered the OC sources in the system: porewater DOC and solid phase TOC. The TOC content  
 612 was ~1 % and decreased with depth in both zones. A decreasing trend over depth was also seen in the DOC  
 613 concentrations. The decrease of OC with depth indicates decomposition and has been commonly observed in other  
 614 studies (Hansen et al., 2017; Mueller et al., 2019). The range in TOC and DOC concentrations are at the lower end of  
 615 comparable ecosystems with the main differences in the upper centimetres (Gribsholt and Kristensen, 2003; Hansen et  
 616 al., 2017; Mueller et al., 2023).

#### 617 4.2 In situ organic carbon manipulation experiment

Deleted: We

Moved (insertion) [1]

Moved up [1]: The few other studies that have detected  $\text{CH}_4$  in the Wadden Sea were at depths where  $\text{SO}_4^{2-}$  was largely depleted (Røy et al., 2008; Wu et al., 2015), which is not the case in our study.

Deleted: is

Deleted: , and could occur, if at all, below

Deleted: using microbial analysis

Deleted: is needed t

Deleted: o

Deleted: fully exclude

Deleted: Collectively, due to the occurrence of Fe(III) reduction (especially in the upper sediment layers) and the availability of  $\text{SO}_4^{2-}$  throughout the sediment, we suggest that electron acceptor availability likely did not limit microbial OC decomposition in our study.

Deleted: ¶

Deleted: Based on the availability of electron acceptors (e.g.,  $\text{SO}_4^{2-}$ ) at all depths and the lack of detectable  $\text{CH}_4$ , we hypothesize that at our field site and other comparable coastal sites, OC is likely the constraint on microbially mediated  $\text{CO}_2$  release and that electron acceptors are likely not a limiting factor. To our knowledge, this is rarely reported for coastal wetlands and not commonly expected for terrestrial ecosystems. Hence, we performed an in situ experiment to test this hypothesis. ¶

#### 644 4.2.1 Validation of the experimental setup

645 Bromide, as an inert tracer, was injected along with the OC/control solution into each experimental cylinder  
646 for each injection cycle. This allowed us to follow the distribution and retention time of the injected solution over one  
647 injection cycle. The Br<sup>-</sup> concentration over each injection cycle was higher than the background Br<sup>-</sup> concentration (Fig.  
648 3/S3a/b), indicating that the injected solution was partially retained within the experimental cylinder over one injection  
649 cycle. The observed decrease in Br<sup>-</sup> concentration over one injection cycle, more pronounced in the intertidal flat (Fig.  
650 S3b), was likely due to flushing out by tidal water and belowground water movement. We observed a slightly lower  
651 retention of Br<sup>-</sup> in the intertidal flats compared to the pioneer zone. We attribute this difference to the higher sand  
652 fraction in the intertidal flats, which likely increased permeability and led to stronger tidal flushing of the injected  
653 solution as well as subject to greater tidal inundation.

654 As the Br<sup>-</sup> concentrations and the respective calculated residual fractions were similar for each cycle (Fig. 3),  
655 we infer that there was no residue of Br<sup>-</sup> and thus no injected OC was carried over between cycles. Furthermore, the  
656 retained Br<sup>-</sup> was similar between the plots of a treatment within one zone, indicating similar belowground conditions  
657 within one zone and thereby validating the experimental setup. By placing the experimental plots outside of vegetated  
658 areas in the pioneer marsh, we tried to avoid geochemical influence on the sediment by plants. However, it is possible  
659 that benthic organisms such as worms may have influenced the biogeochemistry in both the pioneer marsh and  
660 intertidal flat, causing some variability.

#### 661 4.2.2 Effect of organic carbon input in the pioneer marsh

##### 662 Carbon dioxide fluxes

663 To test our hypothesis that that microbially mediated CO<sub>2</sub> release is OC limited in the pioneer marsh, we  
664 injected two different OC sources into the sediment and monitored the subsequent release of CO<sub>2</sub> 1.5, 24, and 48 h post  
665 injection. We observed that acetate treated plots emitted the highest CO<sub>2</sub> throughout the experiment (Fig. 4). No  
666 difference in the CO<sub>2</sub> release was measured between the humic acid treatment and the control despite the additional  
667 availability of OC. This is supported by the work of Gunina and Kuzyakov (2022) who showed that reduced and  
668 complex organics in soils are predominantly thermodynamically preserved due to insufficient energy yield upon  
669 decomposition. Humic acid, as complex OC, may be thus preserved in our study, as reflected in higher DOC  
670 concentrations. In contrast, acetate, with a simpler chemical structure, is favourable for microbial decomposition even  
671 under reducing conditions (Boye et al., 2017; LaRowe and Van Cappellen, 2011) and thus could be readily utilized  
672 and oxidized to CO<sub>2</sub>. Notably, plots treated with humic acid received the same OC concentrations as the acetate plots,  
673 indicating that OC composition is crucial for the CO<sub>2</sub> release from minerogenic pioneer marshes. Based on the  
674 geochemistry at the field site, which suggested that the ecosystem is limited by the availability of OC, the results from  
675 the in situ experiment further support our hypothesis, while simultaneously highlighting the importance of OC  
676 composition. This is contrasting to other terrestrial wetlands, which are characterized by a depletion of TEAs  
677 (Schlesinger and Bernhardt, 2013b).

678 The increased turnover of acetate to CO<sub>2</sub> relative to humic acid is also evidenced in the DOC concentrations  
679 (Fig. S4) and the retention fraction of both DOC sources (Fig. 3a). Although the same mass of OC was added to both  
680 treatments, the DOC concentrations in the acetate plots were significantly lower than that in the humic acid plots,  
681 suggesting that more acetate was utilized, reflected in higher CO<sub>2</sub> release. However, this result does not explain the  
682 lower retention of DOC relative to the retention of Br<sup>-</sup> from the humic acid plots (Fig. 3a). This suggests that in addition  
683 to flushing out, adsorption likely occurred. Previous studies have shown that minerals within the subsurface adsorb  
684 organic compounds (Kahle et al., 2003; Kleber et al., 2021). This adsorption may be preferential, favouring more  
685 aromatic and high molecular weight compounds, particularly when metal (oxyhydr)oxides and clay minerals are  
686 present (Kaiser and Guggenberger, 2000; Lv et al., 2016; Voggenreiter et al., 2024). Based on the results of our study  
687 and a previous study conducted at the same site (Kubeneck et al., 2024), both iron(oxyhydr)oxides and clay minerals  
688 are present. As adsorption suppresses the decomposition of OC (Kleber et al., 2021), we speculate that the lower  
689 retention fraction of humic acid compared to Br<sup>-</sup> was primarily due to adsorption onto the sediment rather than  
690 decomposition. This is consistent with the CO<sub>2</sub> fluxes: humic acid treated plots showed lower retention fractions  
691 compared to the Br<sup>-</sup> retention fractions, however, the CO<sub>2</sub> fluxes were comparable to the control. This suggests that  
692 little to no decomposition occurred and that adsorption was the dominant process. It is worth noting that anoxic  
693 decomposition of humic acid is generally possible but the turnover time would have exceeded the duration of the  
694 experiment (Lipczynska-Kochany, 2018). These results highlight that it is not only the presence of OC that affects  
695 short-term OC release from coastal wetlands; the composition of OC is the primary determining factor.

696 Furthermore, it is important to note that the OC concentrations used in this experiment are higher than those  
697 expected for naturally occurring OC inputs, such as root exudates, which are typically released at lower concentrations  
698 with a continuous input. Thus, upscaling the enhanced CO<sub>2</sub> fluxes measured in our study might result in overestimation  
699 of CO<sub>2</sub> release from minerogenic salt marshes. Our findings rather reveal, on a process level, that the addition of labile  
700 OC stimulates microbially mediated CO<sub>2</sub> release. Enhanced CO<sub>2</sub> release from the acetate amended plots was measured  
701 at nearly all sampling time points (1.5, 24, and 48 h) without a clear trend, while the concentration of the inert tracer  
702 showed a slight decrease over the same period (Fig. S3) – indicating slight dilution and flushing of the injected OC.  
703 This suggest that the elevated CO<sub>2</sub> release was driven by enhanced availability of labile OC independently of its  
704 concentration. These findings allow us to generalize that the system is likely limited by labile OC availability,  
705 regardless of the concentration; however, further work should quantify how the magnitude of CO<sub>2</sub> promotion  
706 corresponds to OC concentration, particularly under low, naturally sustained OC input rates. In conclusion, we can  
707 reliably predict the direction of increased OC inputs to minerogenic salt marshes, but further studies are needed to  
708 predict the specific long-term magnitude of changes in the carbon cycle in these ecosystems.

#### 709 **Enhanced microbial Fe(III) reduction leads to higher CO<sub>2</sub> release**

710 This section combines the observed effect of OC input on the geochemistry of the porewater and sediment  
711 with the microbial growth and metabolic activity and links them to the CO<sub>2</sub> release from the pioneer marsh. The  
712 bacterial 16S rRNA gene copy number, an indicator of the total bacterial abundance, was significantly higher in the  
713 acetate treatment compared to the control for both DNA and RNA at both depths. This suggests greater bacterial  
714 abundance and metabolic activity, which likely led to higher CO<sub>2</sub> fluxes from these plots. No significant difference

715 was noticeable in the 16S rRNA gene copy number between plots amended with humic acid and the control. Overall,  
716 the 16S rRNA gene copy numbers (DNA) are in the range of other studies from coastal wetlands and marine sediment  
717 (Petro et al., 2019; Zhou et al., 2017).

718 The enhanced metabolic activity in the acetate treated plots is further reflected in the elevated aqueous and  
719 solid phase Fe(II). The acetate treatment showed higher aqueous Fe(II) concentrations in all four injection cycles, while  
720 no significant difference was observed between the humic acid and control plots. In the solid phase, the Fe(II) content  
721 was the highest in the acetate treatment. Thus, the higher expression of *Geobacter* spp. in the acetate treated plots  
722 corresponds well to our geochemical observations. *Geobacter* spp. have been shown to use acetate as a carbon source  
723 to gain energy (Coates et al., 1996). The higher Fe(II) levels observed in both aqueous and solid phase of acetate treated  
724 plots along with elevated *Geobacter* spp. gene copies indicate that Fe(III) reduction was stimulated by increased  
725 availability of labile OC.

726 Ferric iron and  $\text{SO}_4^{2-}$  reduction have been reported as OC decomposition processes in salt marshes (Hyun et  
727 al., 2007; Kostka et al., 2002a; Lowe et al., 2000). Sulfide concentrations in the porewater as well as in the solid phase  
728 gave evidence that  $\text{SO}_4^{2-}$  reduction occurred; however, no differences between the treatments and controls were seen.  
729 The functional gene analysis provided further evidence for this, as sulfate-reducing bacteria (SRB) were present  
730 (absolute gene copy numbers in Supplement, Fig. S7); however, none of the treatments led to an increase in their  
731 metabolic activity compared to the control (Fig. 6). Thus, we speculate that the higher  $\text{CO}_2$  release from the acetate  
732 treatment was mainly driven by the enhanced Fe(III) reduction and not by  $\text{SO}_4^{2-}$  reduction. Our finding that acetate is  
733 utilized follows the conventional thermodynamic sequence of iron reduction being more favorable than  $\text{SO}_4^{2-}$  reduction  
734 (Schlesinger and Bernhardt, 2013b) – even if the concentrations and availability of  $\text{SO}_4^{2-}$  were much higher.  
735

### 736 4.2.3 Effect of organic carbon input in the intertidal flat

#### 737 Carbon dioxide fluxes

738 Adding OC to the intertidal flat, a zone more influenced by tides than the pioneer marsh, resulted in CO<sub>2</sub>  
739 trends similar to the pioneer marsh. Acetate addition led to a noticeable increase in CO<sub>2</sub> fluxes. In contrast, the CO<sub>2</sub>  
740 fluxes from the humic acid and control plots were similar. This supports our hypothesis that the electron donor limits  
741 CO<sub>2</sub> release from the ecosystem. Moreover, it highlights that irrespective of tidal influence, the system is limited by  
742 the availability and composition of OC.

#### 743 Enhanced microbial activity leads to higher CO<sub>2</sub> release

744 Total microbial 16S gene copies were significantly higher in the acetate treated intertidal flat plots compared  
745 to the control at both depths (RNA-based), whereas plots amended with humic acid showed no significant difference  
746 from the control plots (Fig. S12a). In contrast to the significant increase in *Geobacter* spp. gene copies, no difference  
747 in the aqueous Fe(II) or in the Fe(II) content in the upper sediment layer (0-5 cm) was measured for the acetate  
748 treatment, except for a higher Fe(II) content in the deeper sediment layer. Conversely, we measured higher AVS  
749 contents in the upper layer for the acetate treatment, but this is not reflected in higher *dsrA* copies numbers. Based on  
750 these mixed results, we consider two hypotheses: (i) acetate promoted increased Fe(III) reduction, which is supported  
751 by higher gene copies of *Geobacter* spp.. However, this is not clearly reflected in the Fe(II) data. Furthermore, with  
752 increased Fe(III) reduction and a constant SO<sub>4</sub><sup>2-</sup> reduction rate, we would have expected a depletion of S(II)<sub>tot</sub> in the  
753 porewater of the acetate treatment due to iron-sulfur mineral formation; however, this was not observed. Thus, we  
754 consider a second hypothesis that (ii) acetate promoted SO<sub>4</sub><sup>2-</sup> reduction, supported by increased AVS content in the  
755 acetate treatment in the upper sediment layer. In contrast, the number of *dsrA* gene copies was not higher in the acetate  
756 treatment. Although a small increase (RNA-based) in the gene copies of *dsrA* was observed in the upper layer, this  
757 was not statistically significant. Additionally, no differences were observed in the S(II)<sub>tot</sub> concentrations, which were  
758 generally low and should therefore be interpreted with caution. Based on our data, we cannot clearly reject either  
759 hypothesis. We therefore suggest Fe(III) and SO<sub>4</sub><sup>2-</sup> reduction both lead to higher CO<sub>2</sub> release, stimulated by higher  
760 supply of labile OC in the intertidal flat.

761 **5 Conclusion and Implications**

762 Our study demonstrated that the composition in combination with the concentration of OC ~~can drive the CO<sub>2</sub>~~  
763 release from minerogenic salt marshes typical of the Wadden Sea. Initial porewater and sediment geochemical  
764 characterization ~~suggested~~ that microbially mediated CO<sub>2</sub> release is likely not limited by the availability of electron  
765 acceptors in both the pioneer marsh and intertidal flat, contrary to what is generally observed in terrestrial wetlands.  
766 Overall, our results indicate that the OC composition, rather than the concentration alone, ~~influenced~~ CO<sub>2</sub> release in  
767 both succession zones. This suggests that OC composition likely plays a limiting role in microbially mediated CO<sub>2</sub>  
768 release from minerogenic salt marshes. ~~We caution here that we did not directly measure TEA reduction rates. Future~~  
769 ~~studies should investigate turnover rates, potentially utilizing isotopes to confirm our findings.~~ The higher CO<sub>2</sub> release  
770 observed in the acetate treated plots within the pioneer marsh was accompanied by higher levels of reduced iron. This  
771 pattern also corresponded with greater activity of Fe(III)-reducing bacteria in these plots, indicating that microbially  
772 mediated CO<sub>2</sub> release resulted from Fe(III) reduction driven by increased labile OC input. The addition of the complex  
773 OC (humic acid) did not exceed the CO<sub>2</sub> release of the control, showing that complex OC was not decomposed. ~~Similar~~  
774 trends in CO<sub>2</sub> release were measured for the intertidal flat, further indicating that OC (both in terms of composition  
775 and concentration) is ~~a key driver of microbial decomposition of OC to CO<sub>2</sub> for salt marsh systems.~~ We expect that  
776 this is particularly relevant in salt marshes similar to ours with a high proportion of fine particles (muddy marshes)  
777 relative to marshes with larger particles (sandy marshes).

778 The results of this in situ study contribute to our understanding of short-term carbon dynamics in minerogenic  
779 temperate salt marshes. Labile OC inputs such as root exudates may enhance CO<sub>2</sub> release from minerogenic salt  
780 marshes, while complex OC inputs, such as plant fragments, might be sequestered in the sediment rather than degraded  
781 and released as CO<sub>2</sub>. The controls on OC turnover observed here should be considered when accounting for these  
782 ecosystems as carbon sinks and stocks. Also, our results show that the link between OC composition and the release  
783 of CO<sub>2</sub>, independent of electron acceptor concentrations, is crucial and should be included in process-based modelling  
784 of carbon fluxes in these ecosystems (Brown, 2025; Regnier et al., 2013). This will contribute to more accurate  
785 predictions of the response of salt marshes to climate change. Further, the in situ experiment simulated a potential  
786 increase of short-term OC inputs to the ecosystem, reflecting scenarios associated with climate change such as  
787 inundation of previously unflooded areas due to sea level rise and storm surges or eutrophication (van Beusekom,  
788 2005; Esselink et al., 2017; Woth et al., 2006). For example, eutrophication may result in an input of organic matter  
789 into the Wadden Sea that is eventually washed onto the coastal sediment. Our study thus provides valuable insight into  
790 the consequences of such short-term scenarios for GHG release and highlights that the input of labile OC (e.g., primary  
791 production during eutrophication, root exudates) into the sediment of a minerogenic salt marsh results in higher CO<sub>2</sub>  
792 releases.

**Deleted:** determines

**Deleted:** indicated

**Deleted:** We caution here that we did not directly measure TEA reduction rates. Future studies should investigate turnover rates, potentially utilizing isotopes to confirm this finding.

**Deleted:** controlled

**Deleted:** Overall, our results indicate that the OC composition, rather than the concentration alone, limits the CO<sub>2</sub> release from minerogenic salt marshes.

**Deleted:** the

804 **CRedit authorship contribution statement**

805 **NK:** Investigation, Methodology, Formal Analysis, Visualization, Writing – Original Draft Preparation,  
806 Conceptualization. **FR:** Investigation, Writing – Review & Editing. **LJK:** Methodology, Writing – Review & Editing.  
807 **RK:** Methodology, Writing – Review & Editing. **AK:** Writing – Review & Editing, Funding Acquisition. **PJ:**  
808 Conceptualization, Funding Acquisition, Supervision, Project Administration, Writing – Review & Editing.

809 **Competing interests**

810 The authors declare that they have no conflict of interest.

811 **Acknowledgements**

812 PJ would like to thank the Ministerium für Wissenschaft, Forschung und Kunst Baden-Württemberg, the University  
813 of Tübingen, and the Deutsche Forschungsgemeinschaft (DFG) for funding through the program Projektförderung für  
814 NachwuchswissenschaftlerInnen. We are grateful for financial support from the Deutsche Forschungsgemeinschaft  
815 (DFG, German Research Foundation, project ID 431072007) and for infrastructural support by the DFG under  
816 Germany's Excellence Strategy, cluster of Excellence EXC2124 (project ID 390838134). LJK and RK were funded  
817 by the European Research Council (ERC) under the European Union's Horizon 2020 research and innovation program  
818 (grant agreement no. 788009-IRMIDYN-ERC-2017-ADG). Furthermore, the authors gratefully acknowledge the  
819 Landesbetrieb für Küstenschutz, Nationalpark und Meeresschutz Schleswig-Holstein and the Nationalpark  
820 Wattenmeer Schleswig-Holstein for permission to conduct our work. For wording and rephrasing in some sections of  
821 the article, an artificial intelligence tool (ChatGPT) was used. We used BioRender to illustrate the experimental setup;  
822 we appreciate their tool. Many thanks to all students, especially to Johanna Isele and Franziska Heitmann, for their  
823 help in the field and laboratory. We are also grateful to Franziska Schädler for her assistance with the molecular biology  
824 analysis. We would like to thank Muammar Mansor for help in the field as well as useful discussions.

825 **Data availability statement**

826 Data are publicly available at Zenodo via [doi.org/10.5281/zenodo.19032950](https://doi.org/10.5281/zenodo.19032950) (Kainz et al., 2025)

827 **References**

- 828 Alongi, D. M.: Carbon Balance in Salt Marsh and Mangrove Ecosystems: A Global Synthesis, *Journal of*  
829 *Marine Science and Engineering*, 8, 767, <https://doi.org/10.3390/jmse8100767>, 2020.
- 830 Arndt, S., Jørgensen, B. B., LaRowe, D. E., Middelburg, J. J., Pancost, R. D., and Regnier, P.: Quantifying  
831 the degradation of organic matter in marine sediments: A review and synthesis, *Earth-Science Reviews*,  
832 123, 53–86, <https://doi.org/10.1016/j.earscirev.2013.02.008>, 2013.
- 833 de Beer, D., Wenzhöfer, F., Ferdelman, T. G., Boehme, S. E., Huettel, M., Van Beusekom, J. E. E., Böttcher,  
834 M. E., Musat, N., and Dubilier, N.: Transport and mineralization rates in North Sea sandy intertidal  
835 sediments, Sylt-Rømø Basin, Wadden Sea, *Limnology and Oceanography*, 50, 113–127,  
836 <https://doi.org/10.4319/lo.2005.50.1.0113>, 2005.
- 837 van Beusekom, J. E. E.: A historic perspective on Wadden Sea eutrophication, *Helgoland Marine*  
838 *Research*, 59, 45–54, <https://doi.org/10.1007/s10152-004-0206-2>, 2005.
- 839 Bosselmann, K., Böttcher, M. E., Billerbeck, M., Walpersdorf, E., Theune, A., Huettel, M., and Jørgensen,  
840 B. B.: Iron-Sulfur-Manganese Dynamics in Intertidal Surface Sediments of the North Sea, *Berichte -*  
841 *Forschungszentrum Terramare*, 12, 32–35, 2003.
- 842 Boye, K., Noël, V., Tfaily, M. M., Bone, S. E., Williams, K. H., Bargar, J. R., and Fendorf, S.:  
843 Thermodynamically controlled preservation of organic carbon in floodplains, *Nature Geoscience*, 10,  
844 415–419, <https://doi.org/10.1038/ngeo2940>, 2017.
- 845 Brown, C. J.: Simulated Biogeochemical Effects of Seawater Restoration on Diked Salt Marshes, Cape Cod  
846 National Seashore, Massachusetts, U.S., *Soil Systems*, 9, 89,  
847 <https://doi.org/10.3390/soilsystems9030089>, 2025.
- 848 BSH: Federal Maritime and Hydrographic Agency, Gezeiten [dataset]. Bundesamt für Seeschifffahrt und  
849 Hydrographie, Hamburg and Rostock, Germany,  
850 [https://gezeiten.bsh.de/friedrichskoog\\_hafen\\_aussenpegel?niveau=nhn](https://gezeiten.bsh.de/friedrichskoog_hafen_aussenpegel?niveau=nhn) [accessed 25.04.2025], 2025.
- 851 Burton, E. D., Bush, R. T., Sullivan, L. A., and Mitchell, D. R. G.: Reductive transformation of iron and  
852 sulfur in schwertmannite-rich accumulations associated with acidified coastal lowlands, *Geochimica et*  
853 *Cosmochimica Acta*, 71, 4456–4473, <https://doi.org/10.1016/j.gca.2007.07.007>, 2007.
- 854 Capooci, M., Seyfferth, A. L., Tobias, C., Wozniak, A. S., Hedgpeth, A., Bowen, M., Biddle, J. F., McFarlane,  
855 K. J., and Vargas, R.: High methane concentrations in tidal salt marsh soils: Where does the methane go?,  
856 *Global Change Biology*, 30, e17050, <https://doi.org/10.1111/gcb.17050>, 2024.
- 857 Cline, J. D.: Spectrophotometric Determination of Hydrogen Sulfide in Natural Waters, *Limnology and*  
858 *Oceanography*, 14, 454–458, <https://doi.org/10.4319/lo.1969.14.3.0454>, 1969.
- 859 Coates, J. D., Phillips, E. J., Lonergan, D. J., Jenter, H., and Lovley, D. R.: Isolation of Geobacter species  
860 from diverse sedimentary environments, *Applied and Environmental Microbiology*, 62, 1531–1536,  
861 <https://doi.org/10.1128/aem.62.5.1531-1536.1996>, 1996.
- 862 Common Wadden Sea Secretariat: Wadden Sea Quality Status Report: Introduction (1.01), Common  
863 Wadden Sea Secretariat, <https://doi.org/10.5281/ZENODO.15195139>, 2017.

864 Cornwell, J. C. and Morse, J. W.: The characterization of iron sulfide minerals in anoxic marine sediments,  
865 *Marine Chemistry*, 22, 193–206, [https://doi.org/10.1016/0304-4203\(87\)90008-9](https://doi.org/10.1016/0304-4203(87)90008-9), 1987.

866 Duarte, C. M., Middelburg, J. J., and Caraco, N.: Major role of marine vegetation on the oceanic carbon  
867 cycle, *Biogeosciences*, 2, 1–8, <https://doi.org/10.5194/bg-2-1-2005>, 2005.

868 Duarte, C. M., Dennison, W. C., Orth, R. J. W., and Carruthers, T. J. B.: The charisma of coastal  
869 ecosystems: Addressing the imbalance, *Estuaries and Coasts*, 31, 233–238,  
870 <https://doi.org/10.1007/s12237-008-9038-7>, 2008.

871 Duarte, C. M., Losada, I. J., Hendriks, I. E., Mazarrasa, I., and Marbà, N.: The role of coastal plant  
872 communities for climate change mitigation and adaptation, *Nature Climate Change*, 3, 961–968,  
873 <https://doi.org/10.1038/nclimate1970>, 2013.

874 van Erk, M. R., Bourceau, O. M., Moncada, C., Basu, S., Hansel, C. M., and De Beer, D.: Reactive oxygen  
875 species affect the potential for mineralization processes in permeable intertidal flats, *Nature*  
876 *Communications*, 14, 938, <https://doi.org/10.1038/s41467-023-35818-4>, 2023.

877 Esselink, P., van Duin, W. E., Bunje, J., Cremer, J., Folmer, E. O., Frikke, J., Glahn, M., de Groot, A. V.,  
878 Hecker, N., Hellwig, U., Jensen, K., Körber, P., Petersen, J., and Stock, M.: Salt marshes. In: Wadden Sea  
879 Quality Status Report 2017, Eds.: Kloepper S. et al., Common Wadden Sea Secretariat, Wilhelmshaven,  
880 Germany. Downloaded 03.11.2024. [qsr.waddensea-worldheritage.org/reports/salt-marshes](https://qsr.waddensea-worldheritage.org/reports/salt-marshes), 2017.

881 Gao, S.: Chapter 10: Geomorphology and Sedimentology of Tidal Flats, in: Coastal Wetlands (Second  
882 Edition), Elsevier, 359–381, <https://doi.org/10.1016/B978-0-444-63893-9.00010-1>, 2019.

883 Gribsholt, B. and Kristensen, E.: Benthic metabolism and sulfur cycling along an inundation gradient in a  
884 tidal *Spartina anglica* salt marsh, *Limnology and Oceanography*, 48, 2151–2162,  
885 <https://doi.org/10.4319/lo.2003.48.6.2151>, 2003.

886 Gunina, A. and Kuzyakov, Y.: From energy to (soil organic) matter, *Global Change Biology*, 28, 2169–  
887 2182, <https://doi.org/10.1111/gcb.16071>, 2022.

888 Hansen, K., Butzeck, C., Eschenbach, A., Gröngröft, A., Jensen, K., and Pfeiffer, E.-M.: Factors influencing  
889 the organic carbon pools in tidal marsh soils of the Elbe estuary (Germany), *Journal of Soils and*  
890 *Sediments*, 17, 47–60, <https://doi.org/10.1007/s11368-016-1500-8>, 2017.

891 Heron, G., Crouzet, C., Bourg, A. C. M., and Christensen, T. H.: Speciation of Fe(II) and Fe(III) in  
892 Contaminated Aquifer Sediments Using Chemical Extraction Techniques, *Environmental Science &*  
893 *Technology*, 28, 1698–1705, <https://doi.org/10.1021/es00058a023>, 1994.

894 Howard, J., Sutton-Grier, A. E., Smart, L. S., Lopes, C. C., Hamilton, J., Kleypas, J., Simpson, S., McGowan,  
895 J., Pessarrodona, A., Alleway, H. K., and Landis, E.: Blue carbon pathways for climate mitigation: Known,  
896 emerging and unlikely, *Marine Policy*, 156, 105788, <https://doi.org/10.1016/j.marpol.2023.105788>, 2023.

897 Huettel, M., Berg, P., and Kostka, J. E.: Benthic Exchange and Biogeochemical Cycling in Permeable  
898 Sediments, *Annual Review of Marine Science*, 6, 23–51, <https://doi.org/10.1146/annurev-marine-051413-012706>, 2014.

900 Hyun, J.-H., Smith, A. C., and Kostka, J. E.: Relative contributions of sulfate- and iron(III) reduction to  
901 organic matter mineralization and process controls in contrasting habitats of the Georgia saltmarsh,  
902 *Applied Geochemistry*, 22, 2637–2651, <https://doi.org/10.1016/j.apgeochem.2007.06.005>, 2007.

903 Jørgensen, B. B., Findlay, A. J., and Pellerin, A.: The Biogeochemical Sulfur Cycle of Marine Sediments,  
904 *Frontiers in Microbiology*, 10, 849, <https://doi.org/10.3389/fmicb.2019.00849>, 2019.

905 Kahle, M., Kleber, M., and Jahn, R.: Retention of dissolved organic matter by illitic soils and clay fractions:  
906 Influence of mineral phase properties, *Journal of Plant Nutrition and Soil Science*, 166, 737–741,  
907 <https://doi.org/10.1002/jpln.200321125>, 2003.

908 Kainz, N., Raab, F., Kubeneck, L. J., Kretzschmar, R., Kappler, A., and Joshi, P.: Carbon dioxide release  
909 driven by organic carbon in minerogenic salt marshes, <https://doi.org/10.5281/zenodo.19032950>, 2025.

910 Kaiser, K. and Guggenberger, G.: The role of DOM sorption to mineral surfaces in the preservation of  
911 organic matter in soils, *Organic Geochemistry*, 31, 711–725, [https://doi.org/10.1016/S0146-](https://doi.org/10.1016/S0146-6380(00)00046-2)  
912 [6380\(00\)00046-2](https://doi.org/10.1016/S0146-6380(00)00046-2), 2000.

913 Kleber, M., Bourg, I. C., Coward, E. K., Hansel, C. M., Myneni, S. C. B., and Nunan, N.: Dynamic  
914 interactions at the mineral–organic matter interface, *Nature Reviews Earth & Environment*, 2, 402–421,  
915 <https://doi.org/10.1038/s43017-021-00162-y>, 2021.

916 Koop-Jakobsen, K., Fischer, J., and Wenzhöfer, F.: Survey of sediment oxygenation in rhizospheres of the  
917 saltmarsh grass - *Spartina anglica*, *Science of The Total Environment*, 589, 191–199,  
918 <https://doi.org/10.1016/j.scitotenv.2017.02.147>, 2017.

919 Kostka, J. E., Roychoudhury, A., and Cappellen, V.: Rates and controls of anaerobic microbial respiration  
920 across spatial and temporal gradients in saltmarsh sediments, *Biogeochemistry*, 60, 49–76,  
921 <https://doi.org/10.1023/A:1016525216426>, 2002a.

922 Kostka, J. E., Gribsholt, B., Petrie, E., Dalton, D., Skelton, H., and Kristensen, E.: The rates and pathways of  
923 carbon oxidation in bioturbated saltmarsh sediments, *Limnology and Oceanography*, 47, 230–240,  
924 <https://doi.org/10.4319/lo.2002.47.1.0230>, 2002b.

925 Kubeneck, L. J., Notini, L., Rothwell, K. A., Fantappiè, G., Huthwelker, T., ThomasArrigo, L. K., and  
926 Kretzschmar, R.: Transformation of vivianite in intertidal sediments with contrasting sulfide conditions,  
927 *Geochimica et Cosmochimica Acta*, 370, 173–187, <https://doi.org/10.1016/j.gca.2024.01.020>, 2024.

928 Kubeneck, L. J., Rothwell, K. A., Notini, L., ThomasArrigo, L. K., Schulz, K., Fantappiè, G., Joshi, P.,  
929 Huthwelker, T., and Kretzschmar, R.: In Situ Vivianite Formation in Intertidal Sediments: Ferrihydrite-  
930 Adsorbed P Triggers Vivianite Formation, *Environmental Science & Technology*, 59, 523–532,  
931 <https://doi.org/10.1021/acs.est.4c10710>, 2025.

932 Kvale, E. P.: The origin of neap–spring tidal cycles, *Marine Geology*, 235, 5–18,  
933 <https://doi.org/10.1016/j.margeo.2006.10.001>, 2006.

934 La, W., Han, X., Liu, C.-Q., Ding, H., Liu, M., Sun, F., Li, S., and Lang, Y.: Sulfate concentrations affect  
935 sulfate reduction pathways and methane consumption in coastal wetlands, *Water Research*, 217,  
936 118441, <https://doi.org/10.1016/j.watres.2022.118441>, 2022.

937 LaRowe, D. E. and Van Cappellen, P.: Degradation of natural organic matter: A thermodynamic analysis,  
938 *Geochimica et Cosmochimica Acta*, 75, 2030–2042, <https://doi.org/10.1016/j.gca.2011.01.020>, 2011.

939 Lipczynska-Kochany, E.: Humic substances, their microbial interactions and effects on biological  
940 transformations of organic pollutants in water and soil: A review, *Chemosphere*, 202, 420–437,  
941 <https://doi.org/10.1016/j.chemosphere.2018.03.104>, 2018.

942 Llobet-Brossa, E., Rabus, R., Böttcher, M., Könneke, M., Finke, N., Schramm, A., Meyer, R., Grötzschel, S.,  
943 Rosselló-Mora, R., and Amann, R.: Community structure and activity of sulfate-reducing bacteria in an  
944 intertidal surface sediment: a multi-method approach, *Aquatic Microbial Ecology*, 29, 211–226,  
945 <https://doi.org/10.3354/ame029211>, 2002.

946 Logemann, E. L., Goesele, C., Jensen, K., and Mueller, P.: Soil Organic Carbon Stocks of German Salt  
947 Marshes: A Comparative Study Along Low- and High-Energy Coastlines, *JGR Biogeosciences*, 130,  
948 e2025JG008797, <https://doi.org/10.1029/2025JG008797>, 2025.

949 Lowe, K. L., Dichristina, T. J., Roychoudhury, A. N., and Van Cappellen, P.: Microbiological and  
950 Geochemical Characterization of Microbial Fe(III) Reduction in Salt Marsh Sediments, *Geomicrobiology  
951 Journal*, 17, 163–178, <https://doi.org/10.1080/01490450050023836>, 2000.

952 Lueder, U., Maisch, M., Laufer, K., Jørgensen, B. B., Kappler, A., and Schmidt, C.: Influence of Physical  
953 Perturbation on Fe(II) Supply in Coastal Marine Sediments, *Environmental Science & Technology*, 54,  
954 3209–3218, <https://doi.org/10.1021/acs.est.9b06278>, 2020.

955 Lueders, T., Manefield, M., and Friedrich, M. W.: Enhanced sensitivity of DNA- and rRNA-based stable  
956 isotope probing by fractionation and quantitative analysis of isopycnic centrifugation gradients,  
957 *Environmental Microbiology*, 6, 73–78, <https://doi.org/10.1046/j.1462-2920.2003.00536.x>, 2004.

958 Lv, J., Zhang, S., Wang, S., Luo, L., Cao, D., and Christie, P.: Molecular-Scale Investigation with ESI-FT-ICR-  
959 MS on Fractionation of Dissolved Organic Matter Induced by Adsorption on Iron Oxyhydroxides,  
960 *Environmental Science & Technology*, 50, 2328–2336, <https://doi.org/10.1021/acs.est.5b04996>, 2016.

961 Maricle, B. R. and Lee, R. W.: Aerenchyma development and oxygen transport in the estuarine  
962 cordgrasses *Spartina alterniflora* and *S. anglica*, *Aquatic Botany*, 74, 109–120,  
963 [https://doi.org/10.1016/S0304-3770\(02\)00051-7](https://doi.org/10.1016/S0304-3770(02)00051-7), 2002.

964 Martens, C. S. and Berner, R. A.: Methane Production in the Interstitial Waters of Sulfate-Depleted  
965 Marine Sediments, *Science*, 185(4157), 1167–1169, 1974.

966 Mcleod, E., Chmura, G. L., Bouillon, S., Salm, R., Björk, M., Duarte, C. M., Lovelock, C. E., Schlesinger, W.  
967 H., and Silliman, B. R.: A blueprint for blue carbon: Toward an improved understanding of the role of  
968 vegetated coastal habitats in sequestering CO<sub>2</sub>, *Frontiers in Ecology and the Environment*, 9, 552–560,  
969 <https://doi.org/10.1890/110004>, 2011.

970 Moeslund, L., Thamdrup, B., and Barker Jørgensen, B.: Sulfur and iron cycling in a coastal sediment:  
971 Radiotracer studies and seasonal dynamics, *Biogeochemistry*, 27, 129–152,  
972 <https://doi.org/10.1007/BF00002815>, 1994.

973 Mueller, P., Ladiges, N., Jack, A., Schmiedl, G., Kutzbach, L., Jensen, K., and Nolte, S.: Assessing the long-  
974 term carbon-sequestration potential of the semi-natural salt marshes in the European Wadden Sea,  
975 *Ecosphere*, 10(1), e02556, <https://doi.org/10.1002/ecs2.2556>, 2019.

976 Mueller, P., Kutzbach, L., Mozdzer, T. J., Jespersen, E., Barber, D. C., and Eller, F.: Minerogenic salt  
977 marshes can function as important inorganic carbon stores, *Limnology and Oceanography*, 68, 942–952,  
978 <https://doi.org/10.1002/lno.12322>, 2023.

979 Nellemann, C., Corcoran, E., Duarte, C. M., Valdés, L., De Young, C., Fonseca, L., and Grimsditch, G.: Blue  
980 Carbon - The Role of Healthy Oceans in Binding Carbon, UNEP. ISBN: 978-82-7701-060-1, 80 pp., 2009.

981 Nolte, S., Koppenaar, E. C., Esselink, P., Dijkema, K. S., Schuerch, M., De Groot, A. V., Bakker, J. P., and  
982 Temmerman, S.: Measuring sedimentation in tidal marshes: a review on methods and their applicability  
983 in biogeomorphological studies, *Journal of Coastal Conservation*, 17, 301–325,  
984 <https://doi.org/10.1007/s11852-013-0238-3>, 2013.

985 Novák, V. and Hlaváčiková, H.: Soil-Water Movement in Water-Saturated Capillary Porous Media, in:  
986 Applied Soil Hydrology, vol. 32, *Springer International Publishing*, Cham, 97–117,  
987 [https://doi.org/10.1007/978-3-030-01806-1\\_8](https://doi.org/10.1007/978-3-030-01806-1_8), 2019.

988 Pendleton, L., Donato, D. C., Murray, B. C., Crooks, S., Jenkins, W. A., Sifleet, S., Craft, C., Fourqurean, J.  
989 W., Kauffman, J. B., Marbà, N., Megonigal, P., Pidgeon, E., Herr, D., Gordon, D., and Baldera, A.:  
990 Estimating Global “Blue Carbon” Emissions from Conversion and Degradation of Vegetated Coastal  
991 Ecosystems, *PLoS ONE*, 7, e43542, <https://doi.org/10.1371/journal.pone.0043542>, 2012.

992 Petro, C., Zäncker, B., Starnawski, P., Jochum, L. M., Ferdelman, T. G., Jørgensen, B. B., Røy, H., Kjeldsen,  
993 K. U., and Schramm, A.: Marine Deep Biosphere Microbial Communities Assemble in Near-Surface  
994 Sediments in Aarhus Bay, *Frontiers in Microbiology*, 10, 758, <https://doi.org/10.3389/fmicb.2019.00758>,  
995 2019.

996 Poffenbarger, H. J., Needelman, B. A., and Megonigal, J. P.: Salinity Influence on Methane Emissions from  
997 Tidal Marshes, *Wetlands*, 31, 831–842, <https://doi.org/10.1007/s13157-011-0197-0>, 2011.

998 R Core Team: R: A Language and Environment for Statistical Computing, R Foundation for Statistical  
999 Computing, Vienna, Austria, <https://www.R-project.org/>, 2025.

1000 Regnier, P., Arndt, S., Goossens, N., Volta, C., Laruelle, G. G., Lauerwald, R., and Hartmann, J.: Modelling  
1001 Estuarine Biogeochemical Dynamics: From the Local to the Global Scale, *Aquatic Geochemistry*, 19, 591–  
1002 626, <https://doi.org/10.1007/s10498-013-9218-3>, 2013.

1003 Revsbech, N. P.: An oxygen microsensor with a guard cathode, *Limnology and Oceanography*, 34, 474–  
1004 478, <https://doi.org/10.4319/lo.1989.34.2.0474>, 1989.

1005 Røy, H., Lee, J. S., Jansen, S., and De Beer, D.: Tide-driven deep pore-water flow in intertidal sand flats,  
1006 *Limnology and Oceanography*, 53, 1521–1530, <https://doi.org/10.4319/lo.2008.53.4.1521>, 2008.

1007 Schlesinger, W. H. and Bernhardt, E. S.: Chapter 5: The Biosphere: The Carbon Cycle of Terrestrial  
1008 Ecosystems, in: Biogeochemistry (3rd edition), Elsevier, Waltham, MA, USA, 135–172,  
1009 <https://doi.org/10.1016/B978-0-12-385874-0.00005-4>, 2013a.

- 1010 Schlesinger, W. H. and Bernhardt, E. S.: Chapter 7: Wetland Ecosystems, in: *Biogeochemistry* (3rd  
1011 edition), Elsevier, Waltham, MA, USA, 233–274, <https://doi.org/10.1016/B978-0-12-385874-0.00007-8>,  
1012 2013b.
- 1013 Seyfferth, A. L., Bothfeld, F., Vargas, R., Stuckey, J. W., Wang, J., Kearns, K., Michael, H. A., Guimond, J.,  
1014 Yu, X., and Sparks, D. L.: Spatial and temporal heterogeneity of geochemical controls on carbon cycling in  
1015 a tidal salt marsh, *Geochimica et Cosmochimica Acta*, 282, 1–18,  
1016 <https://doi.org/10.1016/j.gca.2020.05.013>, 2020.
- 1017 Stookey, L. L.: Ferrozine-a new spectrophotometric reagent for iron, *Analytical Chemistry*, 42, 779–781,  
1018 <https://doi.org/10.1021/ac60289a016>, 1970.
- 1019 Tan, J. H. Y., Mosley, L. M., and Wong, V. N. L.: A Review of Fe–S–C Dynamics in Blue Carbon  
1020 Environments: Potential Influence of Coastal Acid Sulfate Soils, *European Journal of Soil Science*, 76,  
1021 e70047, <https://doi.org/10.1111/ejss.70047>, 2025.
- 1022 Temmink, R., J. M., Lamers, L. P. M., Angelini, C., Bouma, T. J., Fritz, C., van de Koppel, J., Lexmond, R.,  
1023 Rietkerk, M., Silliman, B. R., Joosten, H., and van der Heide, T.: Recovering wetland biogeomorphic  
1024 feedbacks to restore the world’s biotic carbon hotspots, *Science*, 376, 1–7,  
1025 <https://doi.org/10.1126/science.abn1479>, 2022.
- 1026 Tobias, C. and Neubauer, S. C.: Salt Marsh Biogeochemistry - An Overview, in: *Coastal Wetlands: An  
1027 Integrated Ecosystem Approach*, vol. Chapter 16, Elsevier, 539–596, <https://doi.org/10.1016/B978-0-444-63893-9.00016-2>, 2019.
- 1029 Trifunovic, B., Vázquez-Lule, A., Capooci, M., Seyfferth, A. L., Moffat, C., and Vargas, R.: Carbon Dioxide  
1030 and Methane Emissions From A Temperate Salt Marsh Tidal Creek, *Journal of Geophysical Research:  
1031 Biogeosciences*, 125, e2019JG005558, <https://doi.org/10.1029/2019JG005558>, 2020.
- 1032 Van de Broek, M., Vandendriessche, C., Poppelmonde, D., Merckx, R., Temmerman, S., and Govers, G.:  
1033 Long-term organic carbon sequestration in tidal marsh sediments is dominated by old-aged  
1034 allochthonous inputs in a macrotidal estuary, *Global Change Biology*, 24, 2498–2512,  
1035 <https://doi.org/10.1111/gcb.14089>, 2018.
- 1036 de Vlas, J., Mandema, F., Nolte, S., van Klink, R., and Esselink, P.: Nature conservation of salt marshes.  
1037 The influence of grazing on biodiversity, PUCCIMAR report 09., It Fryske Gea, Olterterp, 2013.
- 1038 Voggenreiter, E., Schmitt-Kopplin, P., Thomas Arrigo, L., Bryce, C., Kappler, A., and Joshi, P.: Emerging  
1039 investigator series: preferential adsorption and coprecipitation of permafrost organic matter with poorly  
1040 crystalline iron minerals, *Environmental Science: Processes & Impacts*, 26, 1322–1335,  
1041 <https://doi.org/10.1039/D4EM00241E>, 2024.
- 1042 Wang, J., Hua, M., Cai, C., Hu, J., Wang, J., Yang, H., Ma, F., Qian, H., Zheng, P., and Hu, B.: Spatial-  
1043 Temporal Pattern of Sulfate-Dependent Anaerobic Methane Oxidation in an Intertidal Zone of the East  
1044 China Sea, *Applied and Environmental Microbiology*, 85, e02638-18,  
1045 <https://doi.org/10.1128/AEM.02638-18>, 2019.
- 1046 Woth, K., Weisse, R., and Von Storch, H.: Climate change and North Sea storm surge extremes: an  
1047 ensemble study of storm surge extremes expected in a changed climate projected by four different  
1048 regional climate models, *Ocean Dynamics*, 56, 3–15, <https://doi.org/10.1007/s10236-005-0024-3>, 2006.

1049 Wu, C. S., Røy, H., and De Beer, D.: Methanogenesis in sediments of an intertidal sand flat in the Wadden  
1050 Sea, Estuarine, *Coastal and Shelf Science*, 164, 39–45, <https://doi.org/10.1016/j.ecss.2015.06.031>, 2015.

1051 Zhou, Z., Meng, H., Liu, Y., Gu, J.-D., and Li, M.: Stratified Bacterial and Archaeal Community in Mangrove  
1052 and Intertidal Wetland Mudflats Revealed by High Throughput 16S rRNA Gene Sequencing, *Frontiers in*  
1053 *Microbiology*, 8, 2148, <https://doi.org/10.3389/fmicb.2017.02148>, 2017.

1054